AD-A057 457 BATTELLE COLUMBUS LABS OHIO F/G 7/4
COMPUTATIONAL STUDY OF CHEMICAL REACTION DYNAMICS: QUANTUM STUD--ETC(U)
JUL 78 G WOLKEN DAAG29-76-C-0048
UNCLASSIFIED ARO-13600.2-CX NL

| OF |
AD
AD57457

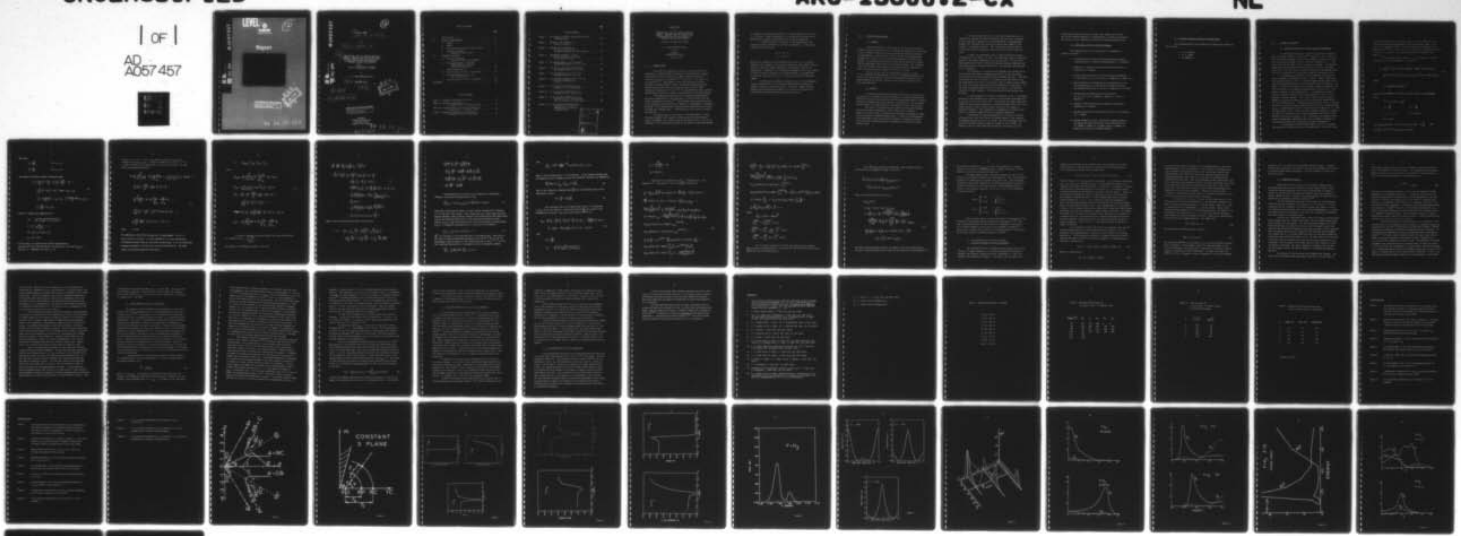

END
DATE
FILMED
9-78
DDC

LEVEL II

Battelle
Columbus Laboratories

12
B.S.

Report

(12)

(9) FINAL REPORT.
1 Jun 76 - 31 May 78

on

(10) George J. Wolken, Jr.

(6) COMPUTATIONAL STUDY OF CHEMICAL REACTION DYNAMICS: QUANTUM STUDY OF SELECTED ATOM-DIATOMIC MOLECULE REACTIONS INVOLVING HYDROGEN, OXYGEN, AND NITROGEN,

(15) Contract No. DAAG29-76-C-0048

to

U. S. ARMY RESEARCH OFFICE

(11) 14 JULY 1978

(12) 55p.

(18) ARO

(19) 13604.2-CX

BATTELLE
Columbus Laboratories
505 King Avenue
Columbus, Ohio 43201

TABLE OF CONTENTS

LIST OF TABLES

Page

LIST OF FIGURES

FINAL REPORT

on

COMPUTATIONAL STUDY OF CHEMICAL REACTION DYNAMICS: QUANTUM STUDY OF SELECTED ATOM-DIATOMIC MOLECULE REACTIONS INVOLVING HYDROGEN, OXYGEN, AND NITROGEN

Contract No. DAAG29-76-C-0048

to

U. S. ARMY RESEARCH OFFICE

from

BATTELLE
Columbus Laboratories

July 14, 1978

I. PROJECT GOALS

There has been considerable progress in recent years in the development of quantum mechanical methods for obtaining state-to-state cross-sections and rate constants for simple chemical reactions.[1] In addition to the H + H_2 reaction,[2,3] results for F + H_2 and H + D_2 have appeared.[4,5] These latter studies have made use of natural collision coordinates (NCC)[6] and of centrifugal decoupling approximations which have been tested by comparison with accurate close-coupling calculations for H + H_2.[4,7] Such approximations make tractable coupled-channel studies of reactions involving atoms other than hydrogen.

The studies mentioned above have utilized an approximation to the kinetic energy which is only applicable to reactions where the most stable configuration is linear.[8] This excludes from consideration most of the bimolecular reactions that are important in mechanisms of combustion processes. Such reactions may be associated with radicals that are stable in highly bent configurations. A representative list is given in Table I (see page 32).

The primary goal of this project is the development of state-of-the-art computer codes capable of studying reactions involving non-linear intermediates on a single adiabatic electronic surface. Due to the complexity of such reactions, stability of the numerical algorithm employed

to integrate the scattering equations is of prime importance, as well as its efficiency. Wyatt's approximation to the NCC kinetic energy will be generalized to include terms important for nonlinear geometries.

A secondary goal of this project is the application of the scattering codes to processes of interest in combustion. Of particular interest are the reactions

$$H + O_2 \rightarrow OH + O$$

$$O + H_2 \rightarrow OH + H$$

which are two important chain-branching steps in the $H_2 - O_2$ reaction, leading to the formation of two product radicals for each reagent radical. The first reaction is highly endothermic, and therefore slow at low temperatures. Knowledge of the temperature dependence of the rate constant for this reaction is necessary for an understanding of low temperature steady-state reactions in the $H_2 - O_2$ system, as well as the explosion regimes.

In addition to providing a theoretical tool for calculating net reaction probabilities, state-to-state probabilities are obtained as immediate results of such calculations. The role of reagent internal energy in determining energy disposal for a reaction can therefore be studied using the methods developed during this project.

II. PROJECT ACCOMPLISHMENTS

A. Summary

During the duration of this project, the natural collision coordinate theory of quantum reactive scattering was generalized to reactions of the form AB+C in which the reaction intermediate could be nonlinear. An approximation to the NCC kinetic energy operator was employed which systematically reduces to that of Wyatt when applied to a linear intermediate. A scattering code developed previously was modified to compute the many additional terms required in the kinetic energy. The resulting code is the present state-of-the-art in the application of quantum reactive scattering theory to general bimolecular reactions.

The new code was tested by application to the $H + H_2$ and $F + H_2$ reactions, and then applied to the $H + O_2$ combustion reaction. As will be seen below, many new results were obtained which should aid our understanding of microscopic processes, many of which are difficult to study experimentally.

B. Details

The quantum mechanical Hamiltonian of Wyatt has been generalized to the case of a nonlinear reaction intermediate. We have determined that additional curvature terms resulting from the noneuclidean nature of natural collision coordinates (NCC) make important contributions to the scattering matrix elements for large deviations from linearity in the reaction zone.

The role of a floating origin originally introduced by Elkowitz and Wyatt has been investigated. We have found that a systematic choice of floating origin can minimize some derivative couplings, and makes little difference in computed probabilities. A choice of switching angle can be made which causes certain matrix elements to identically vanish, but in reactions involving nonlinear intermediates can make other matrix elements large.

The actual physical motion of three interacting atoms was investigated by varying the natural vibrational and rotational coordinates. We have found that a proper choice of NCC parameters can approximately uncouple the vibrational and rotational motions, which simplifies the fitting of the potential surface. This can lead to efficient ways of choosing the points for ab-initio calculations of potential energy surfaces.

Accurate fits were made in NCC to several potential surfaces, including the $H + O_2$ surface of Gauss. This particular system is difficult because of the angular dependence of the reaction path. The use of NCC makes possible the study of correlation diagrams relating vibrational and rotational states of reactants and products, even when the minimum energy path is nonlinear.

Two versions of a scattering code, REACTOR, were tested, one of which utilized the R-matrix propagation procedure of Light and Walker, the other an initial-value method developed by Redmon and Wyatt. Both were satisfactory for the $H + H_2$ and $H + O_2$ reactions, but the R-matrix code was found superior for the $F + H_2$ reaction, with its highly closed channels, due to the way in which inter-sector transformations are constructed. In all cases the R-matrix code was easier to use because of its inherent stability to closed channels. The initial-value code was slightly more efficient.

A study was made of the effect of variation in the $F + H_2$ bending potential on the probability for reaction from the ground vibrational state of H_2 (v=0) into the v=2 state of HF. It was found that simply moving the maximum in the rotational eigenvalue correlation diagram could alter the low energy resonance found for this process, and affect the dynamics of population inversion. This illustrates the importance of reliable calculations of potential energy surfaces for nonlinear geometries.

Calculations of reaction probability as a function of initial vibrational state show that reagent vibrational energy is very effective in promoting reaction in the $H + O_2$ system. This is in agreement with the conclusion of Gauss, based on classical studies of this reaction. An important result is that nonreactive encounters of H with O_2 can form

vibrationally excited O_2, which will then react readily with H atoms. Even at low relative energies, the probabilities for inelastic collisional excitation of O_2 are comparable to the elastic scattering probabilities.

C. Publications Resulting From This Project

The following papers are in preparation for submission to scientific journals:

1. A Generalization of Natural Collision Coordinate Reactive Scattering Theory to Nonlinear Intermediates (A. B. Elkowitz).

2. Kinematics of Reactive Scattering in Natural Collision Coordinates (M. J. Redmon).

3. A Model Potential Surface in Natural Collision Coordinates for the Reaction $H + O_2 \rightarrow OH + O$ (M. J. Redmon and A. Gauss, Jr.).

4. Quantum Mechanical Investigations of the Sensitivity of Reaction Probabilities to Features of the Potential Surface: The Bending Potential for $F + H_2$ (M. J. Redmon and R. E. Wyatt).

5. Quantum Reaction Probabilities for the Reaction $H + O_2 \rightarrow OH + O$ (M. J. Redmon, G. Wolken, Jr., and A. B. Elkowitz).

6. Dynamics of Reactive Scattering in Natural Collision Coordinates (M. J. Redmon).

7. Quantum State-to-State Cross-Sections for the $H + O_2$ Reaction (M. J. Redmon).

8. Quantum Dynamics of the $F + H_2$ Reaction: Resonance Models, and Energy and Flux Distributions in the Transition State (S. Latham, J. McNutt, R. E. Wyatt, and M. J. Redmon, to appear in the Journal of Chemical Physics).

D. Scientific Personnel Supported on This Project

The following Battelle staff members were supported by funds from this contract:

1. A. B. Elkowitz
2. M. J. Redmon
3. G. Wolken, Jr.

III. TECHNICAL DISCUSSION

A. Reactive Scattering in Natural Collision Coordinates

The coordinate system used to describe the reaction dynamics is known as natural collision coordinates.[6] These are a set of center of mass, body fixed coordinates in which Euler angles $\theta\phi\chi$ are used to orient the three particle triangle in space, and three coordinates s, ρ, γ are used to describe the shape of the three particle triangle. In asymptotic regions where the separated atom-molecule limit is valid, s describes translation of the free atom, ρ represents vibration of the diatomic molecule, and γ is rotation of the molecule around the atom-molecule axis.

An abbreviated description of the coordinates as used in the current treatment is presented in Figures 1 and 2. Figure 1 shows only those terms necessary to define a collinear geometry while Figure 2 indicates modifications necessary to include deviation from collinearity. In Figure 1, translation is defined as arc length s along the reference curve (RC), vibrations, ρ, are measured perpendicularly to the RC (i.e., in a plane of constant s), and bending motion, γ, is measured in a plane of constant s around a suitably chosen origin (Figure 2) such that $\gamma=0, \pi$ denotes a collinear geometry. As in previous work, the RC is linear in asymptotic regions and follows the arc of a circle with turning center (TC) in the reaction zone. Following standard practice, the TC is located so that the so-called "schizoid region" occurs in an area of high potential energy. Asymptotically, the RC is chosen to lie at a distance $r = r_c$ from the appropriate Z axis. Unlike previous treatments, however, no reaction path (RP in I) is defined in the collinear geometry since now the intermediate state may be non-linear ($\gamma>0$). Furthermore, for systems of non-linear intermediates, considerably more care is needed in choosing the floating origin (FO) than for systems with linear intermediates.

The existence of a multi-valued region in the $\gamma=0, \pi$ plane is well known and is solved by choice of turning center. A less well known

trouble area exists in the transition region for γ near 90^{o} where the coordinate system becomes overdetermined when the switching angle α is not equal to its asymptotic values. We have introduced a scaled angle γ defined on the intervals $(0, \pi/2)$ and $(\pi/2,\pi)$ such that γ ranges only over the intervals $(0, \gamma_m)$ and $(\pi - \gamma_m,\pi)$ which eliminates the difficulty (see Figure 2).

The classical kinetic energy, T, for a system with a nonlinear intermediate in this approximation is defined by

$$T = \frac{\mu\eta^2}{2}\dot{s}^2 + \frac{\mu}{2}\dot{\rho}^2 + \frac{\mu}{2}r^2\dot{\gamma}^2 + \frac{\mu}{2}R^2\omega_x^2 + \frac{1}{2}(\mu R^2 - \mu r^2 \sin^2\gamma)\omega_y^2 + \frac{1}{2}\mu r^2 \sin^2\gamma\,\omega_z^2 - \mu r^2 f \sin\gamma\cos\gamma\,\omega_y\omega_z - \mu r^2 f\omega_x\dot{\gamma} + \mu r \sin\gamma A_s \dot{s}\omega_x \quad (1)$$

where

$$\mu = (M_a \cdot M_b \cdot M_c / (M_a + M_b + M_c))^{\frac{1}{2}}$$

M_a, M_b, M_c are masses of the three reacting atoms in any arrangement tube.

$$\eta^2 = (1 + \kappa n)^2 + (\kappa_1 m)^2$$

$$\kappa = -\frac{d\Psi}{ds} \qquad \kappa_1 = -\frac{d\alpha}{ds}$$

$$n = r_c - r\cos\gamma \qquad f = \cos(\alpha - \Psi)$$

$$m = r\sin\gamma$$

$$A_s = R_c\kappa_1 \cos(\alpha - \xi) - (1 + \kappa n + \kappa_1 n)\sin(\Psi - \alpha) - f\frac{\partial r_c}{\partial s}, \text{ and}$$

$$R = R_c^2 - r_c^2 + r^2 + 2n(r_c + R_c \sin(\xi - \Psi)).$$

Now using

$$J_i = \frac{\partial T}{\partial \omega_i} \qquad (i = x, y, z)$$

$$P_i = \frac{\partial T}{\partial \dot{q}} \qquad (q = s, \rho, \gamma)$$

one obtains the kinetic energy in momentum terms:

$$2T = \frac{1}{\mu}\frac{g}{Q^2} P_s^2 + \frac{1}{\mu} P_\rho^2 + \frac{1}{\mu}\left[\frac{1}{r^2} + \frac{f^2\eta^2}{Q^2}\right] P_\gamma^2 +$$

$$\frac{1}{\mu}\frac{\eta^2}{Q^2} J_x^2 + BJ_y^2 + CJ_z^2 + fB\cot\gamma\,[J_y, J_z]_+ \qquad (2)$$

$$-\frac{1}{\mu}\left[\frac{r\sin\gamma A_s}{Q^2}\right][J_x, P_s]_+ - \frac{1}{\mu}\frac{fr\sin\gamma A_s}{Q^2}[P_\gamma, P_s]_+ +$$

$$\frac{1}{\mu}\left[\frac{f\eta^2}{Q^2}\right][J_x, P_\gamma]_+$$

where "+" denotes anti-commutator and

$$\mu B = \frac{1}{[R^2 - r^2(\sin^2\gamma + f^2\cos^2\gamma)]}$$

$$C = B\left[\frac{R^2}{r^2\sin^2\gamma} - 1\right]$$

$$Q^2 = \eta^2 g - r^2\sin^2\gamma A_s^2$$

$$g = R^2 - r^2 f^2$$

At this point, we introduce two further approximations.
note that if $s \to -\infty$, then $\Psi \to \pi$ and $\alpha \to 0$ so $\sin(\Psi - \alpha) \to 0$, $\varkappa \to 0$, and $\partial r_c / \partial s \to 0$, thus $A_s \to 0$. Similarly, as $s \to +\infty$, $A_s \to 0$.

Therefore, at s = 0 f = 0 so we approximate the product fA_{s_2} by 0 and eliminate the term $[P_s, P_\gamma]_+$. Secondly we assume that in Q^2, sin $\gamma \rightarrow$ sin γ_o, where "0" denotes the "equilibrium" or reaction path values. We thus obtain the Hamiltonian operator

$$\tilde{H} = \frac{1}{2\mu} \frac{\bar{B}^{-\frac{1}{2}}}{(r_c - \rho)^2 Q_o} \tilde{P}_s \frac{(r_c - \rho)^2}{\bar{B}^{\frac{1}{2}} Q_o} \tilde{P}_s + \frac{1}{2\mu(r_c-\rho)^2 Q_o} \tilde{P}_\rho (r_c - \rho^2) Q_o \tilde{P}_\rho +$$

$$\frac{1}{2\mu} \left[\frac{1}{r^2} + \frac{f^2\eta^2}{Q_o^2}\right] \frac{1}{\sin\gamma} \tilde{P}_\gamma \sin\gamma \tilde{P}_\gamma -$$

$$\frac{1}{2\mu} \frac{\bar{B}^{\frac{1}{2}} \sin\gamma}{r^2 Q_o} \tilde{J}_x \left[\tilde{P}_s \frac{r^3 A_s}{\bar{B}^{\frac{1}{2}} Q_o} + \frac{r^3 A_s}{\bar{B}^{\frac{1}{2}} Q_o} \tilde{P}_s\right] + \tag{3}$$

$$\frac{\eta^2}{2\mu Q_o^2} \tilde{J}_x^2 + \frac{\bar{B}}{2}\tilde{J}_y^2 + \frac{\bar{C}}{2}\tilde{J}_z^2 + fB\cot\gamma [\tilde{J}_y, \tilde{J}_z]_+ +$$

$$\frac{1}{2\mu} \frac{f\eta^2}{Q_o^2} \frac{\tilde{J}_x}{\sin\gamma} [\tilde{P}_\gamma, \sin\gamma]_+ + V(s, \rho, \gamma)$$

where $\bar{B} = \mu B$.

For simplicity, the potential energy may be approximated $V(s,\rho,\gamma) = V_1(s) + V_2(\rho,s) + V_3(\gamma;s)$. In this assumption, V_1 is the translational or minimum potential along the non-linear reaction path, V_2 is the vibrational potential parametric in s and V_3 is the rotational potential. The Hamiltonian is then partitioned into four parts:

$$\hat{H} = \hat{H}_{trans} + \hat{H}_{vib} + \hat{H}_{rot} + \hat{H}_{\rho\gamma s}$$

where

$$\hat{H}_{trans} = \frac{1}{2\mu} \frac{\bar{B}^{\frac{1}{2}}}{(r_c-\rho)^2 Q_o} \tilde{P}_s \frac{(r_c-\rho)^2 g}{\bar{B}^{\frac{1}{2}} Q_o} \tilde{P}_s + V_1(s)$$

$$\hat{H}_{vib} = \frac{1}{2\mu(r_c-\rho)^2 Q_o} \tilde{P}_\rho (r_c-\rho)^2 Q_o \hat{P}_\rho + V_2(\rho;s) \qquad (4)$$

$$\hat{H}_{rot} = \frac{1}{2\mu} \left[\frac{1}{r^2} + \frac{f^2\eta^2}{Q_o^2} \right] \frac{1}{\sin\gamma} \tilde{P}_\gamma \sin\gamma \tilde{P}_\gamma +$$

$$\frac{\eta^2}{2\mu Q_o^2} \tilde{J}_x^2 + \frac{B}{2} \tilde{J}_y^2 + \frac{C}{2} \tilde{J}_z^2 +$$

$$\frac{fB\cot\gamma}{2} [\tilde{J}_y, \tilde{J}_z]_+ + \frac{1}{2\mu} \frac{f\eta^2}{Q_o^2} \frac{\tilde{J}_x}{\sin\gamma} [\tilde{P}_\gamma, \sin\gamma]_+ + V_3(\gamma;s)$$

$$\hat{H}_{\rho\gamma s} = -\frac{1}{2\mu} \frac{\bar{B}^{\frac{1}{2}} \sin\gamma}{r^2 Q_o} \tilde{J}_x \left[\tilde{P}_s \frac{r^3 A_s}{\bar{B}^{\frac{1}{2}} Q_o} + \frac{r^3 A_s}{\bar{B}^{\frac{1}{2}} Q_o} \tilde{P}_s \right]$$

To obtain a symmetric interaction matrix the total wave function is rescaled so that $\Psi = \frac{Q_o^{1/2} \bar{B}^{1/4}}{rg^{1/2}} \Phi$.

This leads to a Schrödinger equation of the form

$$\frac{-\hbar^2}{2\mu}\frac{\partial^2\Phi}{\partial s^2} - \frac{\hbar^2}{2\mu g}\left\{\frac{\partial^2}{Q_o\partial\rho^2}Q_o + \left(\frac{\partial Q_o}{\partial\rho}\right)^2\right\}\Phi$$

$$+ \frac{Q_o^2}{g}\left\{-\frac{\hbar^2}{2\mu}\left[\frac{1}{r^2} + \frac{f^2\eta^2}{Q_o^2}\right]\frac{1}{\text{Sin }\gamma}\frac{\partial}{\partial\gamma}\text{ Sin }\gamma\frac{\partial}{\partial\gamma}\right.$$

$$+ \frac{\eta^2}{2\mu Q^2}\tilde{J}_x^{\,2} + \frac{B}{2}\tilde{J}_y^{\,2} + \frac{C}{2}\tilde{J}_z^{\,2} + \qquad (5)$$

$$\left. + \frac{fB\cot\gamma}{2}\left[\tilde{J}_y,\tilde{J}_z\right]_+ + \frac{1}{2\mu}\frac{f\eta^2}{Q_o^2}\frac{\tilde{J}_x}{\text{Sin }\gamma}\left[\tilde{P}_\gamma,\ \text{Sin }\gamma\right]_+ + \right\}\Phi$$

$$- \frac{1}{2\mu}\frac{Q_o^{1/2}\bar{B}^{1/4}\text{Sin }\gamma}{rg^{1/2}}\tilde{J}_x\left[\tilde{P}_s,\ \frac{r^2A_s}{Q_o^{1/2}\bar{B}^{1/4}g^{1/2}}\right]_+\Phi$$

$$- \frac{\hbar^2}{2\mu}U(s,\rho)\ \Phi$$

$$- \frac{1}{2\mu}\frac{Q_o^{1/2}\bar{B}^{1/4}\text{Sin }\gamma}{rg^{1/2}}\tilde{J}_xQ_o\left[\tilde{P}_s\ \frac{Q_o^{1/2}\bar{B}^{1/4}}{rg^{1/2}}\right]\Phi$$

$$= \left(E - V_1(s) - V_2(\rho;s) - V_3(\gamma;s)\right)\frac{Q_o^2}{g}\Phi$$

where $U(s,\rho)$ is an effective potential with the form

$$U(s,\rho) = \frac{1}{g}\left\{-\frac{1}{2}Q_o\frac{\partial^2Q_o}{\partial\rho^2} - \frac{3}{4}\left(\frac{\partial Q_o}{\partial\rho}\right)^2 + Q_o\frac{\partial Q_o}{\partial\rho}\frac{1}{r_c-\rho}\right\}$$

$$- \frac{3}{4}\frac{1}{Q_o^2}\left(\frac{\partial Q_o}{\partial s}\right)^2 + \frac{1}{2}\frac{1}{Q_o}\frac{\partial^2Q_o}{\partial s^2} - \frac{1}{4}\frac{1}{Q_o}\frac{\partial Q_o}{\partial S}\frac{1}{\bar{B}}\frac{\partial\bar{B}}{\partial S}$$

$$+\frac{1}{Q_o}\frac{\partial Q_o}{\partial \rho}\frac{1}{r_c-\rho}\frac{\partial r_c}{\partial s}+\frac{1}{2Q_o}\frac{\partial Q_o}{\partial s}\frac{1}{g}\frac{\partial g}{\partial s}$$

$$-\frac{5}{16}\frac{1}{\bar{B}^2}\left(\frac{\partial \bar{B}}{\partial s}\right)^2+\frac{1}{4\bar{B}}\frac{\partial^2 \bar{B}}{\partial s^2}+\frac{1}{2\bar{B}}\frac{\partial \bar{B}}{\partial S}\frac{1}{r_c-\rho}\frac{\partial r_c}{\partial s}$$

$$+\frac{1}{4\bar{B}}\frac{\partial \bar{B}}{\partial s}\frac{1}{g}\frac{\partial g}{\partial s}-\frac{1}{r_c-\rho}\frac{\partial^2 r_c}{\partial s^2}-\frac{1}{r_c-\rho}\frac{\partial r_c}{\partial s}\frac{1}{g}\frac{\partial g}{\partial s}$$

$$+\frac{1}{4g^2}\left(\frac{\partial g}{\partial s}\right)^2-\frac{1}{2g}\frac{\partial^2 g}{\partial s^2}$$

The wavefunction Φ is written as an expansion in translation, vibration, and rotation wavefunctions so that

$$\Phi^{JM}_{j_o \ell_o n_o} = \Sigma_{j\ell n}\, T_{j_o \ell_o n_o j\ell n}(s)\; \Omega^{JM}_{j\ell}(\theta\phi\chi\gamma; s)\; H_n(\rho; s) \qquad (6)$$

where JM are good quantum numbers of total angular momentum and Z component of J in the body fixed system. Other indices are j,ℓ,n which label molecular angular momentum, orbital angular momentum, and vibrational energy respectively and are good quantum numbers only in the separated atom-molecule limit. Indices j_o,ℓ_o,n_o label the initial state of the system before reaction begins. $H_n(\rho; s)$, a vibrational wavefunction, is a solution of the equation

$$\frac{\partial^2}{\partial \rho^2} H_n + \frac{2\mu}{h^2}\left\{E_n - V(\rho; s)\right\} H_n = 0 \qquad (7)$$

$\Omega^{JM}_{j\ell}$ is a solution to the rotational part of the Hamiltonian. Note that in the limit of large atom-molecule separation, $A_s=0$ and $Q^2 = \eta^2 g$ so that the Schrodinger equation reduces to that previously used by Wyatt.[8] As before the rotational wavefunction Ω is expanded so that in asymptotic regions

$$\tilde{\Omega}^{JM}_{j_1 \ell_1} = \sum_K N^J_{MK}(\theta\phi\chi)\; \phi^{JK}_{j_1 \ell_1}(\gamma, \pm\pi/2)$$

with

$$\phi^{JK}_{j_1 \ell_1} = \sqrt{2\pi}\ \left(\frac{2\ell_1+1}{2J+1}\right)^{1/2} \langle \ell_1 j_1 0K | JK\rangle\ Y^{K}_{j_1}(\gamma, \pm \pi/2)$$

where + is for products and - is for reactants. As the reaction proceeds and the potential $V_3(\gamma; s)$ becomes non zero the rotational functions are expanded as

$$\Omega^{JM}_{j\ell}(\theta\phi\chi\gamma; s) = \sum_{j_1\ell_1} d^{J}_{j\ell j_1 \ell_1}(s)\ \tilde{\Omega}^{JM}_{j_1\ell_1} \quad . \tag{8}$$

The d's are computed by diagonalizing $\Omega^{JM}_{j\ell}$ over the rotational part of the Hamiltonian so that

$$H_{rot}\ \Omega^{JM}_{j\ell} = W^{J}_{j\ell}\Omega^{JM}_{j\ell} \quad . \tag{9}$$

The rotational part of the Hamiltonian in Eq. (5) is identical to $\hat{H}_{rot}$ in Eq. (4) except it is now multiplied by $\frac{Q_o^2}{g}$ as a result of the wavefunction rescaling. $\hat{H}_{rot}$ may be more simply written as:

$$\hat{H}_{rot} = \frac{A_o}{2}\tilde{J}_x^2 + \frac{B_o}{2}\tilde{J}_y^2 + \frac{C_o}{2}\tilde{J}_z^2 + \frac{E_o}{2}[\tilde{J}_y, \tilde{J}_z]_+ + \frac{fA_o J_x}{2\sin\gamma}[\tilde{P}_\gamma, \sin\gamma] +$$

$$\frac{1}{2}\left[\frac{1}{\mu r^2} + f^2 A_o\right]\frac{1}{\sin\gamma}\ \hat{P}_\gamma \sin\gamma\ \tilde{P}_\gamma + V_3(\gamma; s) \tag{10}$$

with

$$A_o = \frac{\eta^2}{\mu Q_o^2}$$

$$\mu B_o = \frac{1}{R^2 - r^2\ (\sin^2\gamma_o + f^2\cos^2\gamma_o)]}$$

$$C_o = \frac{R^2 B_o}{r^2 \sin^2 \gamma} - B_o$$

$$E_o = f B_o \cot \gamma$$

Equation (9) *is multiplied by* $\phi^{JK}_{j_o \ell_o}$, integrated over γ, and summed over K. This leads to a set of equations of the form:

$$\sum_{j' \ell'} d^J_{j\ell j'\ell'} \left\{ \left[\frac{\hbar^2}{4} (A_o + B_o) J(J+1) + \frac{\hbar^2}{2} \left(\frac{1}{\mu r^2} + f^2 A \right) j'(j'+1) \pm \right.\right.$$

$$\left.\left. \frac{fA\hbar^2}{2} \{J(J+1) + j'(j'+1) - \ell'(\ell'+1)\} - W^J_{j\ell} \right] \delta_{j_o j'} \delta_{\ell_o \ell'} +$$

$$\frac{(2\ell_o+1)^{\frac{1}{2}}(2\ell'+1)^{\frac{1}{2}}}{2J+1} \left[-\frac{(A_o+3B_o)\hbar^2}{4} - fA_o\hbar^2 \right] \sum_K K^2 \langle \ell_o j_o OK | JK \rangle$$

$$\langle \ell' j' OK | JK \rangle \delta_{j_o j'} + \frac{(2\ell_o+1)^{\frac{1}{2}}(2\ell'+1)^{\frac{1}{2}}}{2J+1} \left[-\frac{\hbar^2}{8} (A_o - B_o) \right] \left[2 \sum_{K=3}^{J} \lambda^+_{JK-1} \lambda^+_{JK-2} \right.$$

$$\left[\langle \ell_o j_o\, O\, K-2 | J\, K-2 \rangle \langle \ell' j' OK | JK \rangle \, I^{|K-2|\,|K|}_{j_o j'} + \right.$$

$$\left. \langle \ell_o j_o\, OK | JK \rangle \langle \ell' j'\, O\, K-2 \,|\, J\, K-2 \rangle \, I^{|K|\,|K-2|}_{j_o j'} \right] + \qquad (11)$$

$$\lambda^+_{J0} \lambda^+_{J1} \left[1 + (-1)^{j_o + \ell_o - J} \right] \left[\langle \ell_o j_o\, 00 | J0 \rangle \langle \ell' j'\, 02 | J2 \rangle \, I^{02}_{j_o j'} + \right.$$

$$\left. \langle \ell_o j_o\, 02 | J2 \rangle \langle \ell' j'\, 00 | J0 \rangle \, I^{20}_{j_o j'} \right] - 2(-1)^{j_o + \ell_o - J} \left[\lambda^+_{J0} \right]^2$$

$$\left. \langle \ell_o j_o\, 01 | J1 \rangle \langle \ell' j'\, 01 | J1 \rangle \, I^{11}_{j_o j'} \right\} + \frac{(2\ell_o+1)^{\frac{1}{2}}(2\ell'+1)^{\frac{1}{2}}}{2J+1}$$

$$\left[\frac{R^2 B_o}{r_o^2} - \frac{1}{\mu r^2} - f^2 A_o\right] \sum_K K^2 \langle \ell_o j_o\, OK | JK\rangle \langle \ell' j'\, OK | JK\rangle M_{j_o j'}^{|K|\,|K|} \mp$$

$$\frac{(2\ell_o+1)^{\frac{1}{2}}(2\ell'+1)^{\frac{1}{2}}}{2J+1} \left[\frac{fh^2}{4}(B_o - A_o)\right]\left\{-2 \sum_{K=1}^{J-1} (2K+1)\,\lambda_{JK}^{+}\right.$$

$$[\langle \ell_o j_o\, OK | JK\rangle \langle \ell' j'\, 0\,K+1 | J\,K+1\rangle J_{j_o j'}^{|K|\,|K+1|} +$$

$$\left.\langle \ell_o j_o\, 0\,K+1 | J\,K+1\rangle \langle \ell' j'\, OK | JK\rangle J_{j_o j'}^{|K+1|\,|K|}\right] - \lambda_{J0}^{+}\left[1+(-1)^{j_o+\ell_o-J}\right]\left[\langle \ell_o j_o\, 00 | J0\rangle\right.$$

$$\left.\langle \ell' j'\, 01 | J1\rangle J_{j_o j'}^{01} + \langle \ell_o j_o\, 01 | J1\rangle \langle \ell_o j_o\, 00 | J0\rangle J_{j_o j'}^{10}\right]\Big\} +$$

$$\sum_K \langle \phi_{j_o \ell_o}^{JK} | V_{3(\gamma;s)} | \phi_{j'\ell'}^{JK}\rangle_\gamma \Big\} = 0$$

where

$$\lambda_{JK}^{\pm} = [J(J+1) - K(K\pm 1)]^{\frac{1}{2}}$$

$$I_{j_o j'}^{|K||K'|} = \int P_{j_o}^{|K|} P_{j'}^{|K'|}\, d\cos\gamma$$

$$M_{j_o j'}^{|K||K'|} = \int P_{j_o}^{|K|} \frac{1}{\sin^2\gamma} P_{j'}^{|K'|}\, d\cos\gamma$$

$$J_{j o j'}^{|K||K'|} = \int P_{j_o}^{|K|} \cot\gamma\, P_{j'}^{|K'|}\, d\cos\gamma$$

Once the terms in Equation (11) have been computed, this equation may be solved by diagonalization. This yields both the rotational wavefunctions $\omega_{j\ell}^{JM}(\theta\phi\chi\gamma;s)$ and the energies $W_{j\ell}^{J}(s)$.

With $\Omega^{JM}_{j\ell}$ and H_n having been determined, close coupling equations describing local propagation through a sector are

$$\sum_{nj\ell} \left\{ \delta_{n_1 n}\, \delta_{j_1 j}\, \delta_{\ell_1 \ell} \frac{\partial^2}{\partial s^2} T^J_{j_o \ell_o n_o j \ell n}(s) + V^J_{n_1 j_1 \ell_1\, nj\ell}(s)\, T_{j_o \ell_o n_o\, j\ell n}(s) \right\} = 0 \tag{12}$$

where the interaction matrix is given by

$$\begin{aligned} V_{n_1 j_1 \ell_1}(s) = & \\ & + \langle H_{n_1} \mid U(s,\rho) \mid H_n \rangle_\rho\, \delta_{j_1 j} \delta_{\ell_1 \ell} \\ & + \Big\langle \Omega^{JM}_{j_1 \ell_1} H_{n_1} \Big| \frac{1}{h^2} \left\{ \frac{Q_o^{\frac{1}{2}} B^{\frac{1}{4}} \mathrm{Sin}\gamma}{r\, g^{\frac{1}{2}}} \mathcal{J}_x \left[P_{\gamma_1} \frac{r\, A_s}{Q_o^{\frac{1}{2}} B^{\frac{1}{4}} g^{\frac{1}{2}}} \right]_+ \right. \\ & \left. - \frac{Q_o^{\frac{1}{2}} B^{\frac{1}{4}} \mathrm{Sin}\gamma}{r\, g^{\frac{1}{2}}} \mathcal{J}_x Q_o \left[\tilde{P}_s \frac{Q_o^{\frac{1}{2}} B^{\frac{1}{4}}}{r_o g^{\frac{1}{2}}} \right] \right\} \Big| \Omega^{JM}_{j\ell} H \Big\rangle_{\theta\phi\chi\gamma\rho} \\ & + \frac{2\mu}{\hbar^2} \left[W^J_{j\ell}(s) + \frac{1}{2} \left(E_n(s) + E_n(s) \right) + V_1(s) - E \right] x \\ & \langle H_{n_1} \mid \frac{Q_o^2}{g} \mid H_n \rangle_\rho\, \delta_{j_1 j} \delta_{\ell_1 \ell} \quad . \end{aligned} \tag{13}$$

The usual first-derivative term does not appear, since we are anticipating the use of locally adiabatic basis functions and intersector transformations.[5]

Once the matrix elements $V_{j_1 \ell_1 n_1 \ell n}(s)$ have been generated, the coupled equations are solved via the Magnus method. Boundary conditions are then applied to obtain the scattering probabilities.

The above equations may be partially decoupled by the use of so-called J_z-conserving or coupled-states approximations. This is an essential procedure for applications to systems other than $H + H_2$. The calculation presented in this report employed the decoupling approximation of Wyatt,[7] so that calculations for $J>0$ involve no more coupled equations than $J=0$. Instead of the triangle inequality, values of j, ℓ for $J>0$ are determined by the prescription

$$J \text{ even} \quad \begin{cases} j = \text{odd} & \ell = |J-j| \\ j = \text{even} & \ell = \begin{cases} J \text{ if } j \leq J \\ j \text{ if } j > J \end{cases} \end{cases}$$

$$J \text{ odd} \quad \begin{cases} j = \text{odd} & \ell = |J-j| \\ j = \text{even} & \ell = \begin{cases} J \text{ if } j \leq J \\ j + 1 \text{ if } j > J \end{cases} \end{cases}$$

These relations result in proper bifurcation of the hindered rotor functions at the boundary separating reactants and products.[7,9] This type of decoupling in NCC has been shown to be remarkably effective for $H + H_2$, where comparison with accurate close-coupling is possible.[4,7] This success is partly due to the use of a switching angle to reorient the Z-axis from reactants to products during the reaction.

B. The Representation of Potential Energy Surfaces in Natural Collision Coordinates

The convenience of NCC in studying reactive systems arises from the use of a single variable, s, to follow the system from reactants to products, and internal (vibration-rotation) coordinates ρ, γ that vary smoothly from reactants to products. s is taken to be the position on a

reference curve defined in the collinear plane corresponding to an instantaneous position of the system point representing the reacting molecules. It is through the potential energy decomposition

$$V(s,\rho,\gamma) = V_1(s) + V_2(\rho;s) + V_3(\gamma;s) + V_4(\rho,\gamma;s) \qquad (15)$$

that the concept of a reaction path is introduced. V_1 is defined by specifying $\rho_o = r_c - r_o$ and γ_o in a constant s-plane. By connecting the values of V_1 obtained in this manner and plotting them as a function of s we obtain a "reaction path potential" connecting reactants and products, i.e., a potential energy correlation diagram for the adiabatic electronic state of interest. Since (ρ,γ) are orthogonal coordinates, once V_1 is specified, V_2 and V_3 then represent stretching and bending potentials for displacements away from the NCC equilibrium geometry (s, ρ_o, γ_o). V_4 is required to make the decomposition exact, and represents vibration-rotation interaction in the potential energy, which for some systems is small in NCC. This representation of the potential surface is very convenient because the translational, vibrational and rotational potentials can often be represented by simple analytic functions. This simplifies studies of the effects of potential surface variation on the dynamics of a chemical reaction. The separate analytic functions defining vibration and rotation represent collective motions of the three-atom system, similar to normal coordinates. For $H + H_2$ at $s = 0$ the motions in NCC correspond to normal coordinates.

It is convenient to choose V_2^o and V_3^o to be potentials such that the resulting hamiltonians for internal motion are easily soluble. This is because we need eigenfunctions of internal motion to expand the scattering wavefunction. By choosing these potentials to combine with kinetic energy terms to give Morse oscillator and hindered asymmetric top hamiltonians, we then have a decomposition

$$V(s,\rho,\gamma) = V_1(s) + V_2^o(\rho;s) + V_3^o(\gamma;s) + V_4^o(\rho,\gamma;s) \qquad (16)$$

where V_4 is now given by

$$V_4 = V_4 + (V_2 - V_2^o) + (V_3 - V_3^o) \qquad (17)$$

We have found that Morse and hindered rotor eigenfunctions are very useful representations to use in calculations. Other choices of representation, such as harmonic oscillators and free rotors, allow rapid calculation of matrix elements, but result in a much larger interaction matrix in the scattering equations, since they do not represent the vibrational and rotational motions as well. They have advantages in some applications, however, particularly the harmonic oscillator functions, since they can be used to aid convergence when continuum vibrational states play a role in the scattering. Since harmonic oscillator functions and corresponding matrix elements are much less time consuming to compute than those of Morse oscillators, convergence tests and studies of step-size variations are more efficiently performed with these simpler functions.

The quantities necessary to define the NCC representation of the potential surface are the path potential V_1, and quantities parametric in s used to define the model potentials for internal motion. These are r_o and γ_o (obtained when V_1 is determined), α_m, the local Morse exponent, and a functional representation of the local bending potential. In Figures 3 to 5 we illustrate the variation of V_1, r_o, γ_o, and α_m for several reactions. Cubic splines are used to represent the curves. There are two particularly useful forms for the bending potential. The simple form

$$V_3^o(\gamma) = \frac{Vo}{2}(1-\cos\ 2\gamma) \tag{18}$$

and the much more flexible Legendre expansion

$$V_3^o(\gamma) = \sum_n C_n P_n(\cos\ \gamma) \tag{19}$$

The coefficients $\frac{Vo}{2}$ and C_n are parametric in s, and vary smoothly from reactants to products. We have employed the first form extensively for our $F + H_2$ calculations. The second form is required for a realistic representation of a system with a bent intermediate. In Figure 6 we show a fit of $\frac{Vo}{2}$ for $F + H_2$. In Figure 7 we show a Legendre fit to the local bending

potential for $H + O_2$ taken from the potential surface of Gauss. It should be noted that the motion of the three atom system in NCC depends on the choice of floating origin and switching angle. Thus the potential fits will vary with this choice.

C. Computational Aspects

Apart from the representation of the potential energy surface, scattering calculations can be considered in three separate steps. First, the matrix elements appearing in the coupled equations must be computed. Second, the equations must be integrated along the reaction coordinate to obtain a global solution. Finally, the physical solution is obtained by the application of appropriate boundary conditions.[10]

For the calculations presented in this report, we have neglected vibration-rotation coupling in the potential, i.e., we set $V_4 = 0$. This is consistent with our treatment of the kinetic energy, and allows us to vary the vibrational and rotational parts of the problem independently. It should be pointed out that this pertains to NCC only; the internuclear coordinates are still coupled in a cartesian space.

Since we use a vibrational basis of Morse oscillators all vibrational matrix elements must be evaluated numerically. We use standard Simpson quadrature formulas for this purpose. The rotational matrix elements are determined analytically in a basis of free rotors, and the hindered rotor functions are then obtained by diagonalization using at present a Jacobi algorithm. The time required to obtain both vibrational and rotational matrix elements for a system like $H + O_2$ is about 1000 CP seconds on a CDC 7600, assuming 16 vibrational states with 20 rotational levels. We have found it more efficient to discard the basis functions and retain only the matrix elements used for scattering. This is because of the large amount of space required to store the numerical functions. The matrix elements are computed once, and used for all energies, and for all angular momenta if centrifugal decoupling is employed.

Two versions of the scattering code, REACTOR, were employed. The first, an initial-value method using basis sets that do not vary within a

small region (sector) along the reaction coordinate, using the exponential sector transformation of Redmon and Wyatt. This method had been previously applied to the H + H_2, H + D_2, and F + H_2 reactions,[5] and represents the sector overlap matrix required for the transformation as

$$\underset{\sim}{S} = e^{-i\delta\hat{P}_s/\hbar} \approx e^{-i\delta\underset{\sim}{\hat{P}}_s/\hbar} \tag{20}$$

This use of the translation operator requires that we compute the energy-independent first derivative matrix $\underset{\sim}{P}_s$. It should be noted that we are making an approximation, in representing a matrix exponential as the exponential of a matrix, that becomes exact in the limit of a complete basis. Since $\underset{\sim}{P}_s$ is antisymmetric and traceless, $\underset{\sim}{S}$ is orthogonal, and flux is conserved across sector boundaries. Furthermore, using the Light-Walker method of wavefunction scaling[11] with the sector method described above (i.e., without explicitly including first and second derivative couplings) results in a symmetric interaction matrix. One would expect then that a unitary $\underset{\sim}{S}$-matrix would result, and this is what we observe. In most instances total probability is unity to seven or eight digits.

The main difficulty with this procedure is the assumption of completeness used in the exponential matrix evaluation. Excellent results were obtained for H + H_2, but F + H_2 presented difficulties in trying to achieve convergence, although the probabilities themselves appeared reasonable. We therefore modified REACTOR by using the Light-Walker R-matrix propagation method.[12] All matrix element evaluations were the same, except that instead of using the exponential transformation method, requiring first-derivatives, direct numerical overlaps are used. This generally is expected to degrade flux conservation when an incomplete basis is used, but because of the way in which the transformation is constructed in the R-matrix method, i.e., by replacing matrix inverses by transposes (again, this is exact in the limit of a complete basis) flux is satisfactorily conserved. In our F + H_2 calculations using the R-matrix method, flux was conserved to a few tenths

of one percent. While this is not as impressive as the conservation obtained with the exponential sector transformations, it is satisfactory. The R-matrix method appears more stable with respect to convergence of the vibrational basis. There is no apparent reason why the exponential method and the R-matrix method should have the same rate of convergence, and in fact our difficulty with the exponential transformation may stem from the slow convergence of our representation of the matrix of the translation operator. It is apparently much slower for $F + H_2$ than the rate of convergence of the coupled-channel expansion of the wavefunction.

The initial-value method is inherently unstable to closed channels. In practice, one observes that total probabilities of unity can be obtained if closed-channels are not carried to asymptotic limits of the reaction coordinate, but are picked up and dropped at appropriate places during the course of the integration. Experience has taught us how to do this effectively. The R-matrix method does not have this difficulty, and closed channels can be carried to asymptotic regions. We feel that the sensitivity of the initial value approach to closed-channels can be viewed in a positive light, since when conservation is achieved one can perhaps feel confident about the stability of the integration. Because closed channels are not carried to asymptotic limits, our current implementation of the initial value method is somewhat more efficient than our R-matrix code. However, there is no reason why the R-matrix method cannot be similarly coded.

Most of the applications presented in this report were obtained using the R-matrix version of REACTOR. The most time consuming calculations involved the 60 channel runs for $F + H_2$, carried out on the CDC 6600 at the University of Texas at Austin in collaboration with Professor Wyatt. We used 280 steps over the reaction coordinate, and typical execution times were 1500 CP seconds per E and J. We could have saved time by using 200 steps, with only slight loss in accuracy. Most of the time is spent in matrix multiplication and diagonalization routines. A Jacobi method was used for diagonalization, and is known to be inefficient for large matrices. Code development currently in progress (including optimum step-size selection) should enable us to obtain similar results in about 600-800 CP seconds. This

corresponds to about 100 CP seconds per E, J on a CDC 7600. This means that the information required to obtain reliable state-to-state rate constants for reactions like $F + H_2$, $O + H_2$ and $H + O_2$ can be obtained for a few hours of computation on a CDC 7600.

D. Recent Results for the $F + H_2$ Reaction

The R-matrix version of REACTOR has been applied to the $H + H_2$ reactions, and reaction probabilities are in good agreement with results obtained previously.[4,5] An extensive set of calculations were undertaken to study the effects of varying the bending potential, V_3, on computed reaction probabilities. This type of investigation is expected to yield information concerning the importance of nonlinear configurations in determining the product energy disposal from reactive encounters. Similar collinear quantum calculations investigated the effects of variation of the $F + H_2$ vibrational potential on reaction probabilities.[13] It was found that the presence of wells in the adiabatic vibrational correlation diagram were responsible for the low-energy population inversion observed in the reactive probability curves. These wells are associated with the local expansion of the collinear potential surface in the downhill part of the reaction path. This is reflected in a drop in the value of the local Morse exponent used to define the vibrational potential, and indicates that an accurate knowledge of the features of the potential surface in this region is crucial for obtaining state-to-state reaction probabilities.

A model potential of the form given by Equation (18) was used for the bending potential in these investigations. We first represented $\frac{Vo}{2}$ by the simple parametric form

$$\frac{Vo}{2} = \frac{A}{e^{-BX}+e^{BX}} \tag{21}$$

where $X = |s-s_{max}|$. By varying the parameters in the expression, the hindered rotor eigenvalues obtained with the potential of Equation (18) can be made to have a maximum value at $s = s_{max}$. A is chosen so that the lowest

(j=0) eigenvalue has a preselected maximum. We initially chose this value to correspond to the zero-point bending energy of the Muckerman II F + H_2 surface.[14] Two values were used for s_{max}, s = 0.49 corresponding to the F + H_2 saddle point on the Muckerman V surface,[15] and s = 0 corresponding to a point on the downhill part of the reaction path. The latter value was chosen because by placing the maximum in the bending zero-point energy at a value of s where both the potential V_1 and the vibrational energy are dropping rapidly (i.e., we are going into a vibrational well) we expect to minimize the effect of the bending energy on the reaction dynamics. A final modification of the bending potential, now being used in extensive calculations, is to replace equation 21 with a locally determined fit to $\frac{Vo}{2}$ which reproduces the j = 0 eigenvalue for the Muckerman V surface at many values of s. This should allow us to model the dynamics on this surface rather well. It should be mentioned that the reason for not using an accurate Legendre expansion such as Equation (19) is our desire to eliminate the complication of the V_4 term in the potential, and a V_3 of the form of Equation (19) results in a bending potential that is much too hard, requiring that V_4 be included in order that the rotational eigenvalues should not be too large.

The extensive results we are getting for this system are to be published in the scientific literature,[16] and therefore will only be briefly discussed here. Our calculations for this particular study involve 10 vibrational states, and up to 12 rotational states in the 4 open product vibrational levels, for a total of 60 coupled channels. Previous work has shown that this basis is sufficiently converged for our purpose. In Figure 8 we attempt to represent in perspective the information that is directly obtained from calculations of this type. Scattering probabilities are obtained as a function of total angular momentum J and total energy E, from which it is possible to obtain cross-sections and finally rate constants. We show in this figure the probability for ground state H_2 reacting with F atoms to produce vibrationally excited HF in V' = 2. This figure corresponds to s_{max} = 0 in Equation (21). The low energy probability curve for J = 0 (vs. E) shows a pronounced maximum around .34 eV. Going out in total J (at this energy) the probability monotonically decreases. If we choose a higher energy and scan out in total J, we notice instead that the probability rises to a

maximum at a nonzero value of J before exhibiting monotonically decreasing behavior. The explanation for this lies in the shape of the J = 0 probability vs energy. The sharp maximum at .34 eV is the result of a Feshbach resonance process[13] involving quasibound states associated with wells in the distortion potentials mentioned above. For J>0, the probability curves (vs E) are similar, but the onset of resonance behavior occurs at higher total energy than at J = 0 due to the shift of reaction threshold. These are quantum effects, and total cross-sections from our previous calculations indicate that they are not completely removed by averaging.[1,5]

In Figure 9 the probabilities are shown in more detail for two energies. In Figure 10 the probabilities are plotted for J = 0 and J = 10 as a function of energy. Also shown in these figures are probabilities for reaction into the V' = 3 manifold of HF.

Calculations in which $s_{max} = 0.49$ result in very small reaction probabilities for J = 0. One maximum of .07 occurs at .35 eV, with another of .08 at .43 eV. The reaction probabilities are thus drastically altered by moving the maximum in $\frac{Vo}{2}$ along the reaction path. With this potential, we find a large reaction probability only for J>0, where we again observe the resonance behavior in the probabilities.

The first 3-D quantum calculations that we reported for $F + H_2$[4] were made with a very limited rotor basis (2 rotors per vibrational level) and an integration method that explicitly included first and second derivatives of the basis functions. These results showed the population inversion into V' = 2 of HF, and subsequent work has verified the essential correctness of the probability curves reported there. We have performed similar calculations using the present model bending potential, with $s_{max} = 0$. The results are shown in Figure 11, and are not significantly altered from the results of Ref. 4, even though the bending potential in that case was an expansion of the form

$$V_3(\gamma) = \frac{1}{2}Vo(s)(1-\cos 2\gamma) + A(s)\sum_{n=0}^{10} C_n P_n(\cos\gamma) + B(s) \qquad (22)$$

in which the Legendre coefficients were fixed at one value of s (to set the shape of the potential) with Vo, A and B determined locally. These studies

indicate that qualitatively correct reaction probabilities for vibrational processes may be obtained for some systems with severely truncated rotor bases.

Currently we are using a V_3 given by Equation (18) with $\frac{Vo}{2}$ as shown in Figure 6 in an extensive study of the F + H_2 reaction, in which state-to-state reaction rates will be the end result.

E. Reaction Probabilities for the H + O_2 Reaction

We have applied the code REACTOR to the H + O_2 reaction using a fit to the modified LEPS surface of Gauss.[17] A vibrational basis of up to 16 Morse oscillators was used with a limited rotational basis of only 2 hindered rotors, in the spirit of our early F + H_2 calculations.[4] Preliminary results for vibrationally excited O_2 reacting to produce ground state OH indicate that vibrational energy is very efficient in promoting the reaction. This is in agreement with the classical trajectory results of Gauss.[17] We have attempted to determine the convergence of the coupled channel expansion, but we are presently limited by code dimensions to about 70 channels, and the behavior observed so far indicates we will need over 100. Flux conservation is usually better than 1% for the calculations reported here. When we tried to increase the rotational basis, flux conservation deteriorated rapidly, due to mixing, and probably will not improve until many more states are used. A modified version of the program employing extended core storage will be used for calculations with a larger basis. This will allow us to investigate the role of reagent rotational energy on the scattering.

In Figure 12 we present reaction probabilities for H + O_2(v) at 1.0 eV total energy. It is evident that reagent vibrational energy is very effective in promoting reaction. Comparisons of these figures with similar results for F + H_2 in Figure 9 show significant differences in the dynamics between the two reactions. The H + O_2 probability curves have more structure, probably indicative of complexing associated with the deep well in the surface. In contrast, the F + H_2 curves are relatively simple.

In Table II we present some probabilities for H + O_2(v=4, j=0) at several energies and total angular momenta. The structure indicated by the

diversity in magnitude of these results illustrates the complexity we generally find in the energy variation of the scattering probabilities. By contrast, the F + H_2 probabilities are quite smooth. Because of this structure, it will be necessary to solve the coupled equations over a rather fine energy grid.

We find that reaction from v=0 in O_2 is small, but not negligible. Gauss found essentially no classical trajectories that were reactive when starting out in v=0. It is likely that some of his trajectories that were labeled as complex would actually have led to reaction if he could have followed them to completion. He was not able to do this because of numerical difficulties encountered in trying to integrate such trajectories.

Another interesting feature of the reaction is the difference between the v=4 curve and the curves for v=2 and v=3 in Figure 12. The v=4 curve grows gradually and has a very broad maximum, while the others drop to a low value at relatively small J. This indicates that the large cross-sections found for v>4 may be associated with dynamical effects that are quite different than occur when less vibrational energy is available. Gauss ran only a few trajectories for v<4 and these gave no reaction. It would be useful to see if trajectories for v<4 might indicate a more direct mechanism, with less complexing.

F. Cross-Sections for the H + O_2 Reaction

The probabilities discussed in the preceding section have been used to estimate total cross-sections for H + O_2 at 1.0 eV total energy. These are presented in Table III. Gauss reported a value of about .35 $\AA^2$ for the v=4 vibrational state of O_2. He estimates that his value could be as much as a factor of 10 too small, a result of his inability to follow complex trajectories. Our quantum cross-section is about 10 times larger than his, which is consistent with his estimate of the number of complex trajectories that might lead to reaction. It is necessary for us to obtain cross-sections at other energies before a rate-constant can be determined for this reaction. The rate-constants obtained by Gauss are lower than experiment, and the larger cross-sections that seem to be resulting from the quantum scattering are evidently going to improve this, although the threshold behavior will have to be carefully investigated.

In Table IV we present some inelastic (nonreactive) partial cross-sections Q^J which indicate that inelastic $H + O_2$ encounters tend to produce vibrationally excited O_2, which in turn can react rapidly with hydrogen. This could complicate the analysis of experiments in which state-selection is not employed.

The LEPS potential surface used for these calculations does not produce the known force constants for HO_2, and since these calculations were begun, Gauss has modified the surface to reproduce these force constants to about 20%.[18] In addition, an extensive ab-initio surface obtained with large-scale CI calculations has become available.[19] This latter surface should be employed in any extensive studies of the $H + O_2$ reaction.

REFERENCES

1. For a review of recent reaction coordinate scattering results including a fairly extensive bibliography see R. E. Wyatt, Quantum Mechanics of Neutral Atom-Diatomic Molecule Reactions, in State-to-State Chemistry, P. R. Brooks and E. F. Hayes, eds., ACS Symposium Series 56 (American Chemical Society, Washington, D.C., 1977.

2. G. Wolken and M. Karplus, J. Chem. Phys. 60, 351 (1974).

3. (a) G. C. Schatz and A. Kuppermann, J. Chem. Phys. 62, 2502 (1975); 65, 4642 (1976); 65, 4668 (1976); (b) A. B. Elkowitz and R. E. Wyatt, J. Chem. Phys. 63, 702 (1975); 62, 2504 (1975).

4. M. J. Redmon and R. E. Wyatt, Int. J. Quantum Chem. Symp. 9, 403 (1975).

5. M. J. Redmon and R. E. Wyatt, Int. J. Quantum Chem. Symp. 11, 343 (1977).

6. R. A. Marcus, J. Chem. Phys. 49, 2610 (1968).

7. A. B. Elkowitz and R. E. Wyatt, Mol. Phys. 31, 189 (1976).

8. R. E. Wyatt, J. Chem. Phys. 56, 390 (1972).

9. S. H. Harms and R. E. Wyatt, J. Chem. Phys. 62, 3162 (1975); 62, 3173 (1975); A. B. Elkowitz and R. E. Wyatt, J. Chem. Phys. 62, 3683 (1975).

10. J. C. Light, Methods in Computational Physics, Vol. 10, B. Alder and M. Rotenberg, Eds. (Academic Press, New York, 1971).

11. J. C. Light and R. B. Walker, J. Chem. Phys. 65, 1598 (1976).

12. J. C. Light and R. B. Walker, J. Chem. Phys. 65, 4272 (1976).

13. S. Latham, J. McNutt, R. E. Wyatt, and M. J. Redmon, J. Chem. Phys. (in press).

14. J. T. Muckerman, J. Chem. Phys. 56, 2997 (1972).

15. Parameters for the Muckerman V surface are given by G. C. Schatz and A. Kuppermann, J. Chem. Phys. 63, 674 (1975).

16. M. J. Redmon and R. E. Wyatt, Quantum Mechanical Investigations of the sensitivity of reaction probabilities to features of the potential surface: The bending potential for F + H_2 (to be published).

17. A. Gauss, Jr., J. Chem. Phys. 68, 1689 (1978).

18. A. Gauss, private communication.

19. C. Melius, private communication.

Table I - Combustion Reactions of Interest

$$H + O_2 \rightarrow OH + O$$

$$O + H_2 \rightarrow OH + H$$

$$O + N_2 \rightarrow ON + N$$

$$N + O_2 \rightarrow NO + O$$

$$B + OH \rightarrow BO + H$$

$$B + O_2 \rightarrow BO + O$$

$$C + O_2 \rightarrow CO + O$$

$$C + OH \rightarrow CO + H$$

$$CN + O \rightarrow CO + N$$

Table II - Reaction Probabilities for

$H + O_2(v=4, j=0) \rightarrow O + OH(v=0, j=all)$

E_{TOTAL} (eV)	J=0	5	10	15	20
.85	.161	.143	.080	0.	0.
.90	.002	.236	.023	.093	.020
.95	.097	.013	.491	.040	.007
1.00	.113	.249	.406	.083	.004
1.05	.090				
1.10	.146				

Table III - Cross Sections for
$H + O_2(v,j=0) \rightarrow O + OH(v=0, j=all)$
at 1.0 eV total energy

v	E_{rel} (eV)	Q_{vo} (Å^2)
0	.903	.16
1	.711	.26
2	.522	.30
3	.338	.77
4	.159	3.40

Table IV - Nonreactive partial cross-sections*
for $H + O_2(v=0;\ j=0) \rightarrow H + O_2(v,j=all)$

v	.85eV, J=5	.9eV, J=10	1.0eV, J=16
0	.01	.11	.09
1	.15	.15	.17
2	.08	.06	.12
3	.05	.24	.38
4	.04	.03	.09

* Values are in $Å^2$.

FIGURE CAPTIONS

Figure 1 — The natural coordinate representation of the collinear plane. The reaction coordinate s is measured along the reference curve RC, with s=0 corresponding to its intersection with SS. Also shown is a planar reaction path.

Figure 2 — Deviation from linearity in a plane of constant s. The region between γ_m and the m-axis must be avoided to avoid double-counting of spatial configurations of the 3-atom system.

Figure 3 — Reaction Path potentials for $H + H_2$, $F + H_2$, and $H + O_2$ obtained from empirical LEPS surfaces.

Figure 4 — Exponential parameter α used to define local Morse potentials for $F + H_2$ and $H + O_2$.

Figure 5 — The bending angle γ_o and scaled NCC equilibrium distance r_o which define the reaction path for the $H + O_2$ reaction.

Figure 6 — A local fit to $\frac{Vo}{2}$ used to parametrize the bending potential for $F + H_2$.

Figure 7 — Ten-term Legendre fits to the local bending potential for $H + O_2$, shown for three values of s.

Figure 8 — A perspective representation of the P_{02} reaction probability for $F + H_2$ as a function of both E and J.

Figure 9 — $F + H_2$ reaction probabilities as a function of J at two energies.

FIGURE CAPTIONS

Figure 1 The natural coordinate representation of the collinear plane. The reaction coordinate s is measured along the reference curve RC, with s=0 corresponding to its intersection with SS. Also shown is a planar reaction path.

Figure 2 Deviation from linearity in a plane of constant s. The region between γ_m and the m-axis must be avoided to avoid double-counting of spatial configurations of the 3-atom system.

Figure 3 Reaction Path potentials for $H + H_2$, $F + H_2$, and $H + O_2$ obtained from empirical LEPS surfaces.

Figure 4 Exponential parameter α used to define local Morse potentials for $F + H_2$ and $H + O_2$.

Figure 5 The bending angle γ_o and scaled NCC equilibrium distance r_o which define the reaction path for the $H + O_2$ reaction.

Figure 6 A local fit to $\frac{Vo}{2}$ used to parametrize the bending potential for $F + H_2$.

Figure 7 Ten-term Legendre fits to the local bending potential for $H + O_2$, shown for three values of s.

Figure 8 A perspective representation of the P_{02} reaction probability for $F + H_2$ as a function of both E and J.

Figure 9 $F + H_2$ reaction probabilities as a function of J at two energies.

Figure 10 $F + H_2$ reaction probabilities as a function of E for J=0 and J=10.

Figure 11 $F + H_2$ reaction probabilities as a function of E for J=0, obtained with a truncated rotational basis.

Figure 12 $H + O_2$ reaction probabilities as a function of J for E=1.0 eV, obtained with a truncated rotational basis.

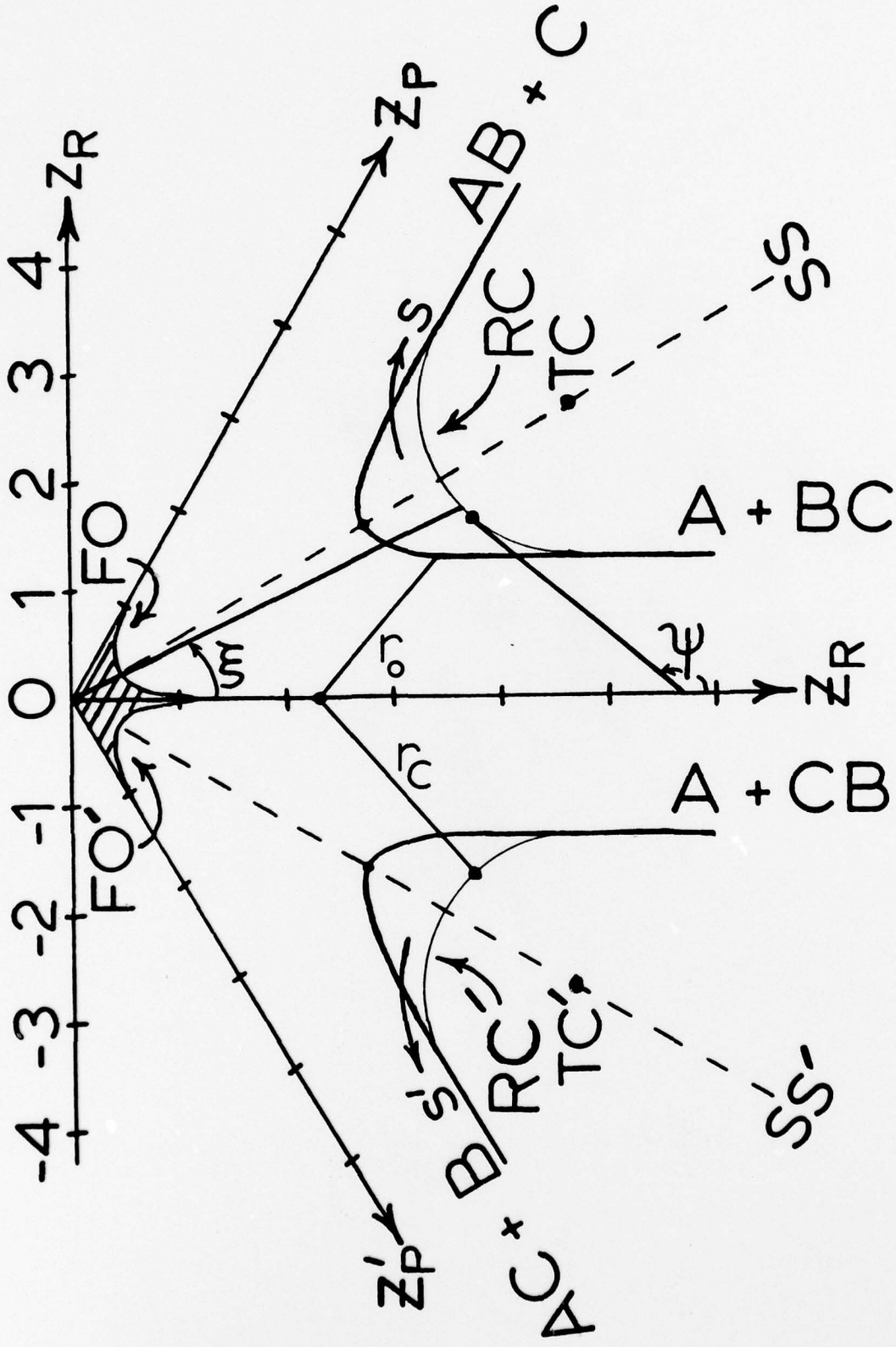
Z_R
Z_P
AB + C
SS
S
RC
TC
4
3
2
1
FO
A + BC
ξ
r_o
ψ
Z_R
O
r_c
A + CB
-1
FO'
-2
-3
-4
Z'_P
B + C
S'
RC'
TC'
SS'

Figure 1

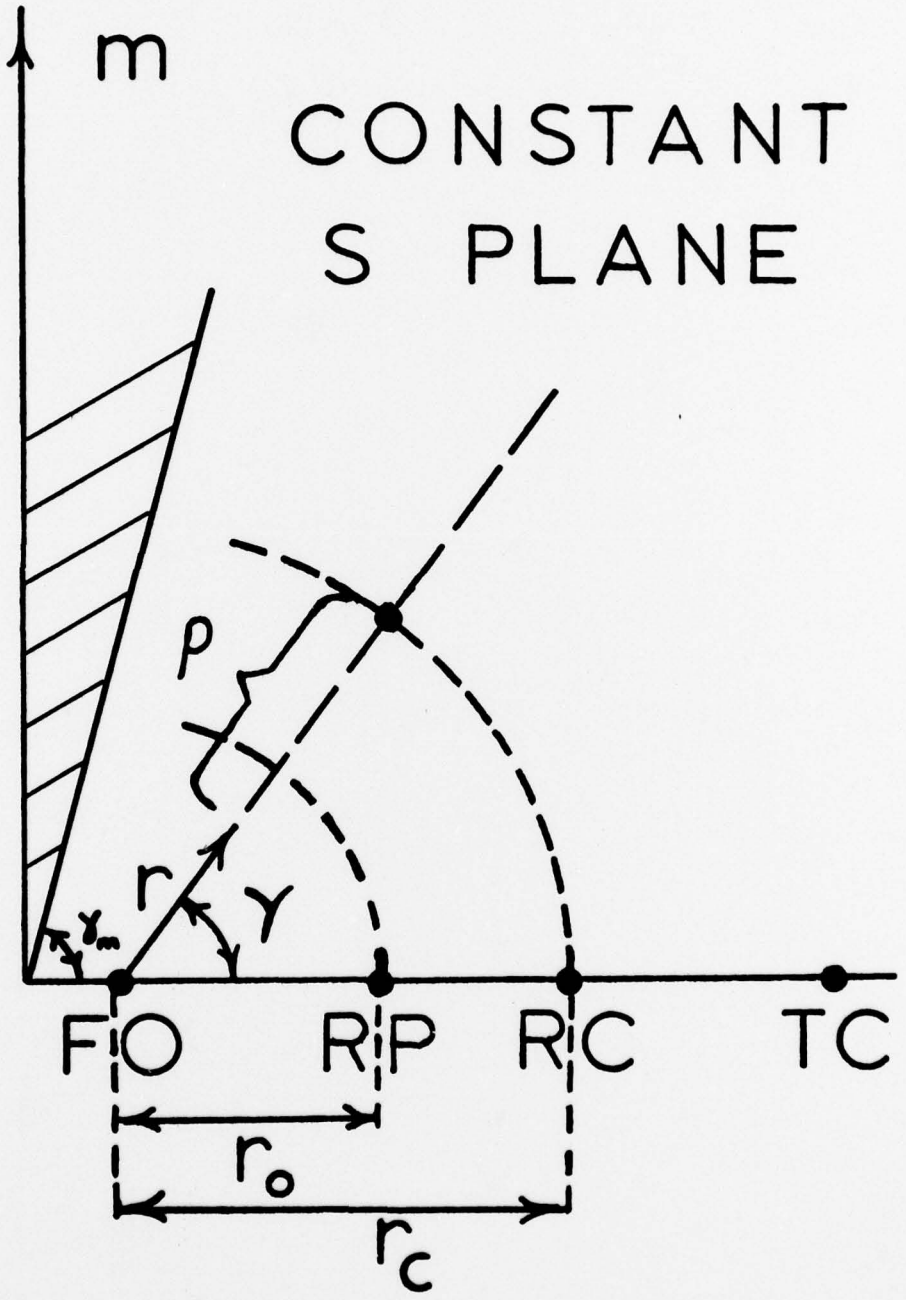

Figure 2

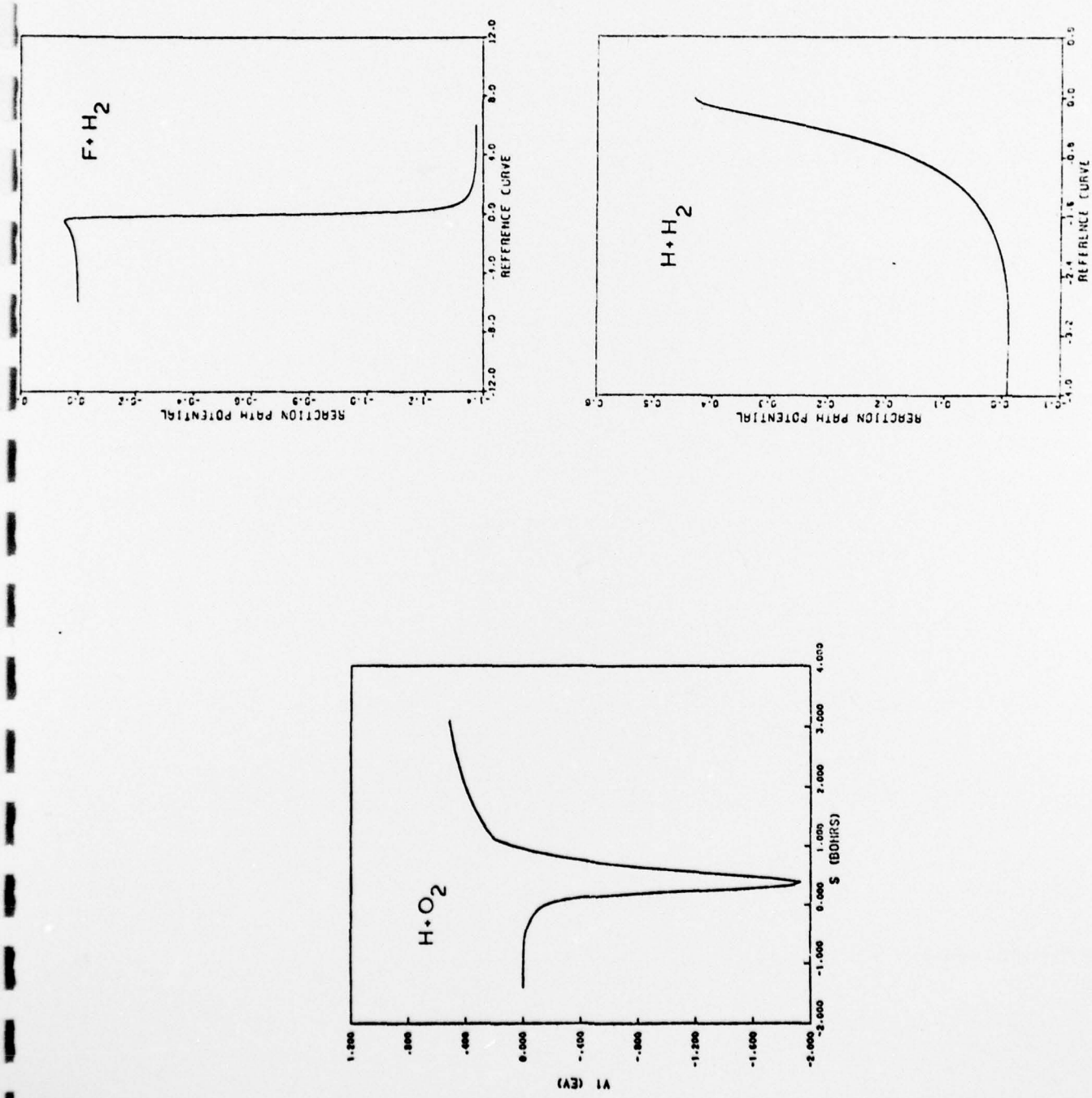
F + H2
REACTION PATH POTENTIAL
REFERENCE CURVE
H + H2
REACTION PATH POTENTIAL
REFERENCE CURVE
H + O2
V1 (EV)
S (BOHRS)

Figure 3

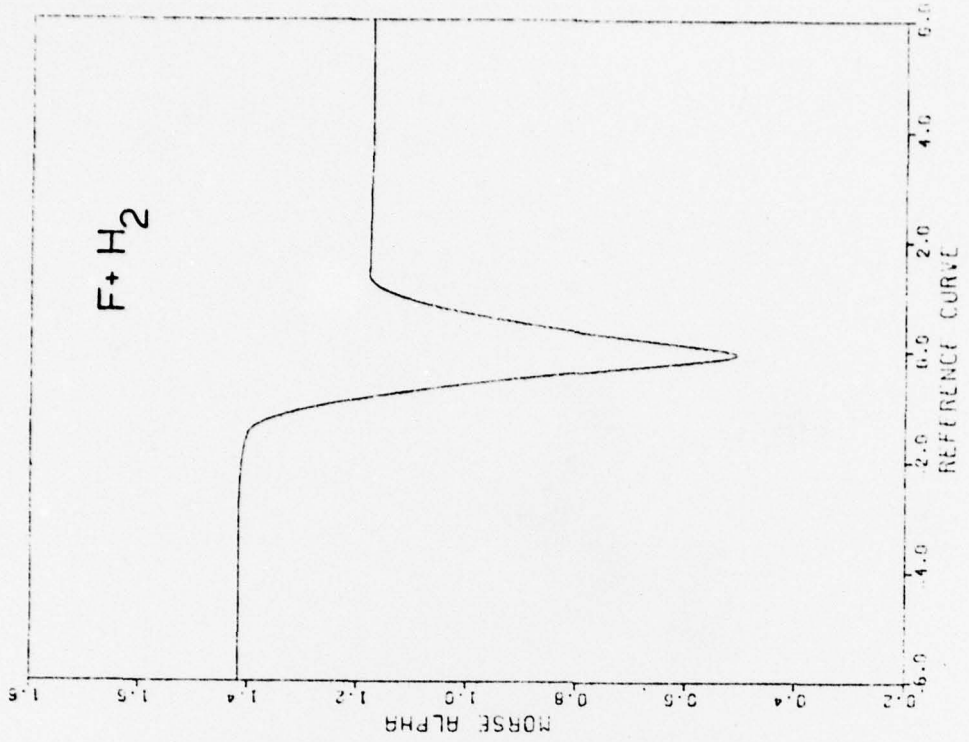

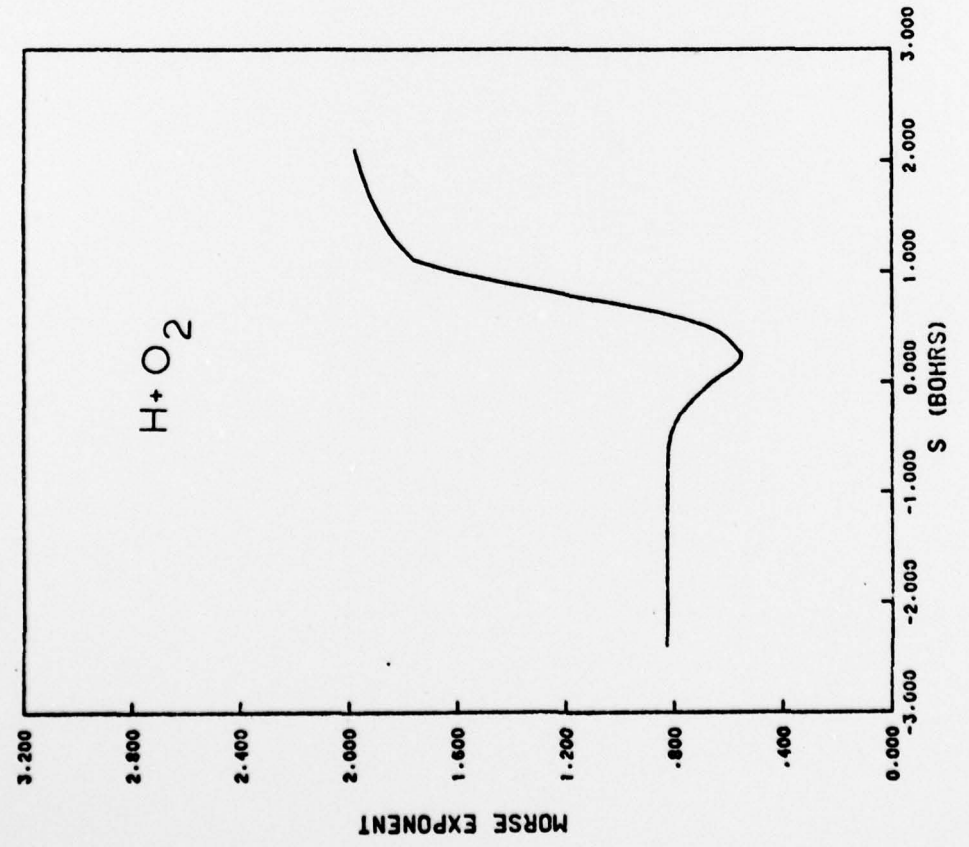

Figure 4

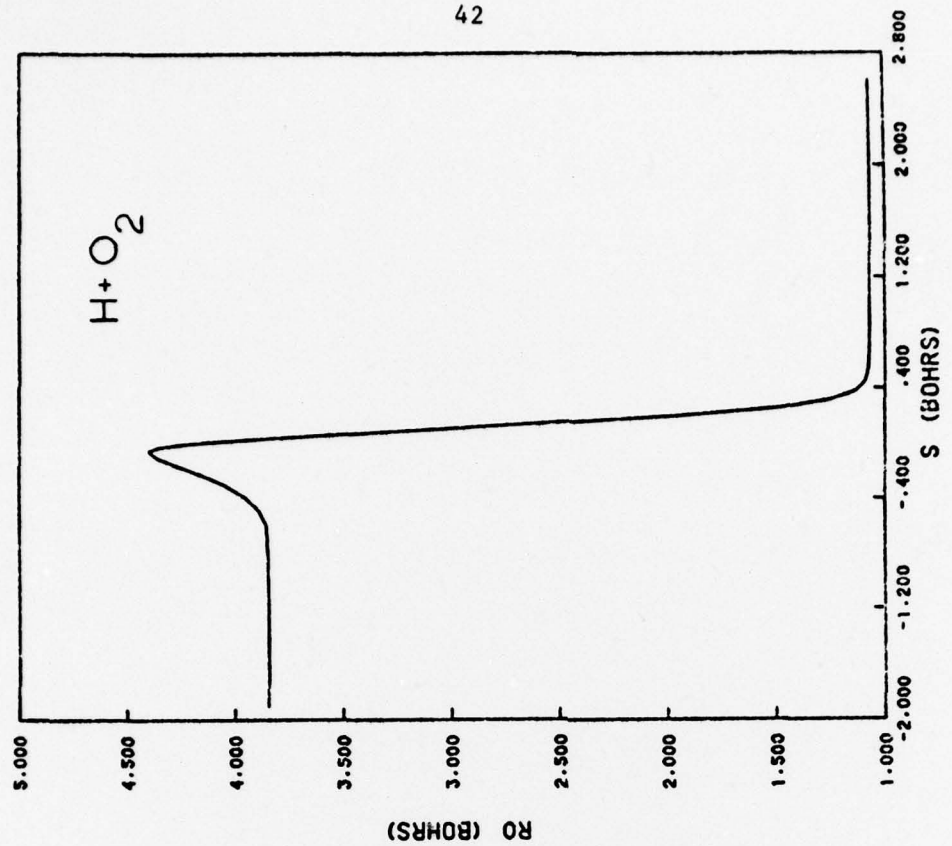
H+O2
RO (BOHRS)
S (BOHRS)
5.000
4.500
4.000
3.500
3.000
2.500
2.000
1.500
1.000
-2.000
-1.200
-.400
.400
1.200
2.000
2.800

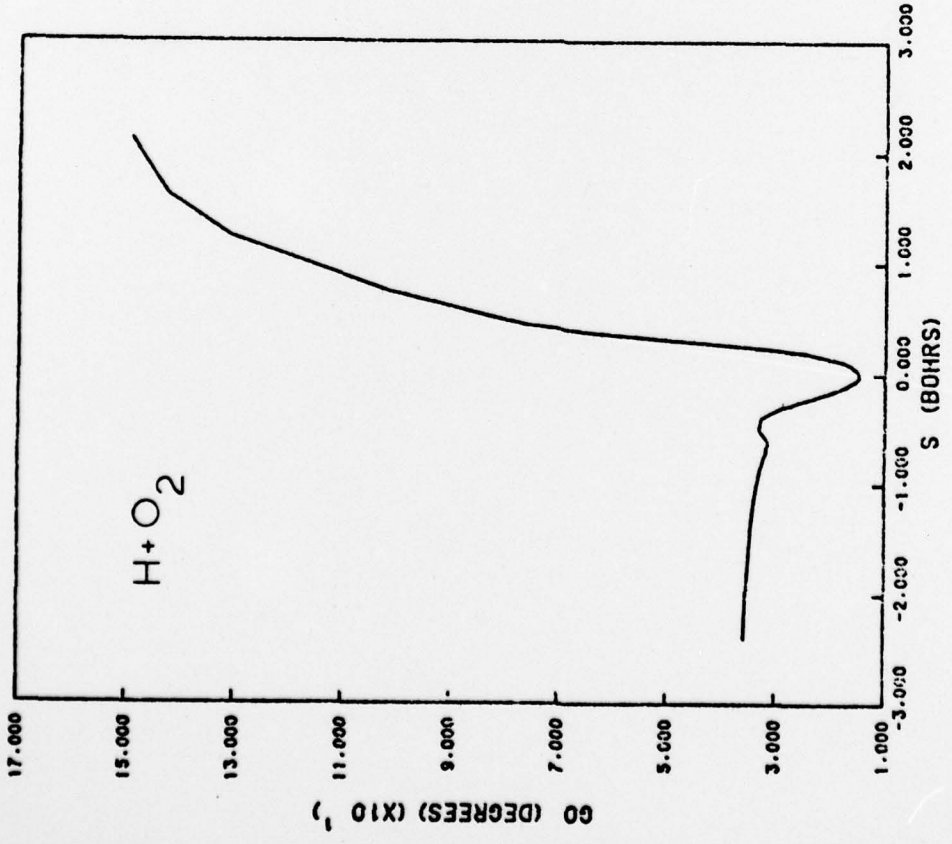
H+O2
GO (DEGREES) (X10)
S (BOHRS)
17.000
15.000
13.000
11.000
9.000
7.000
5.000
3.000
1.000
-3.000
-2.000
-1.000
0.000
1.000
2.000
3.000

Figure 5

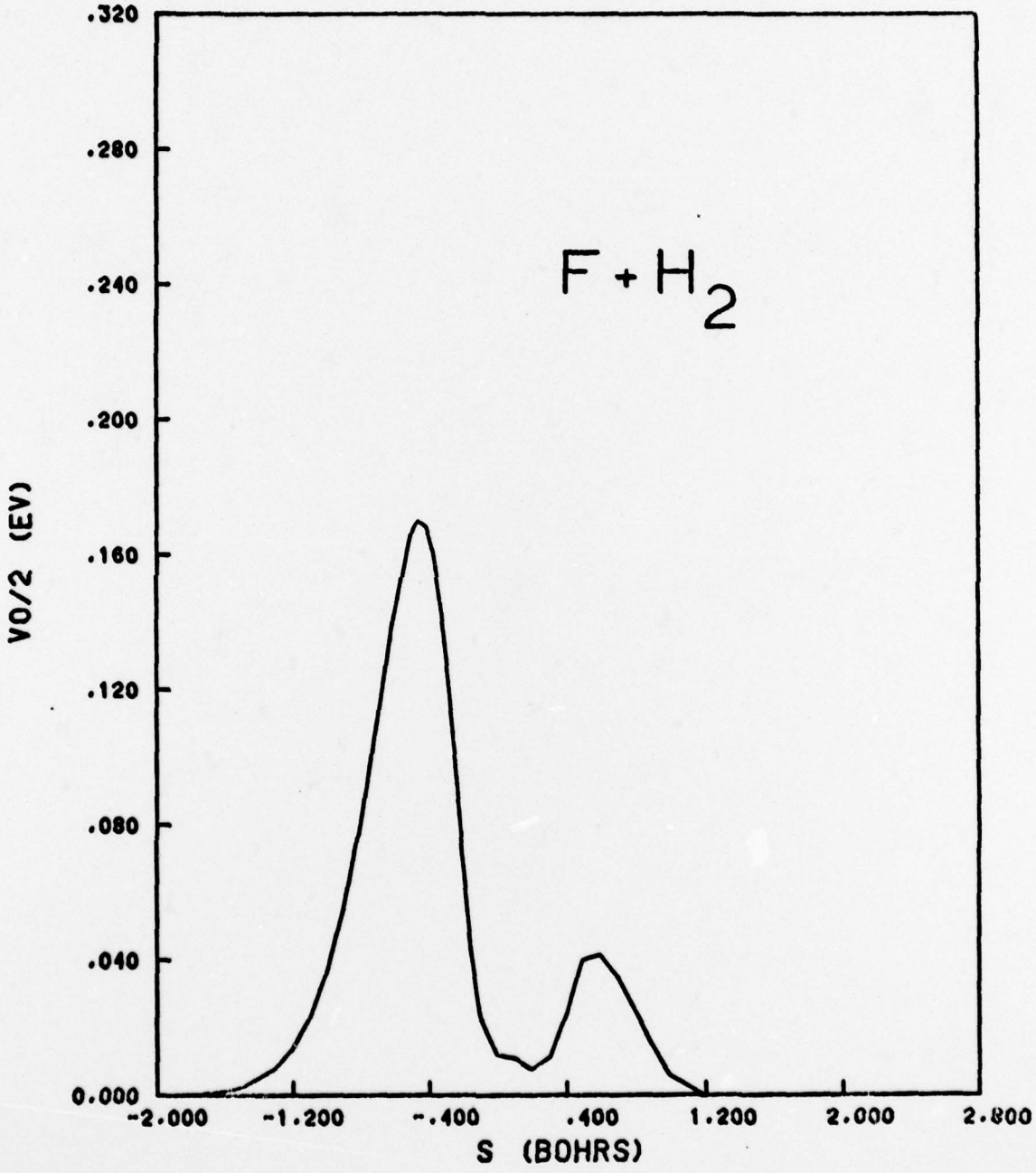
.320
.280
.240
.200
.160
.120
.080
.040
0.000
V0/2 (EV)
F + H2
-2.000
-1.200
-.400
.400
1.200
2.000
2.800
S (BOHRS)

Figure 6

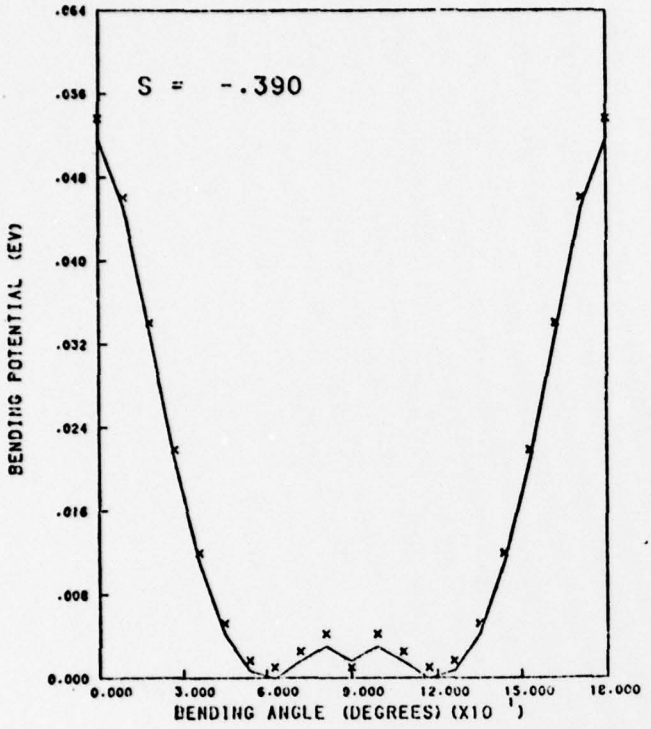
S = -.390
BENDING POTENTIAL (EV)
.064
.056
.048
.040
.032
.024
.016
.008
0.000
0.000
3.000
6.000
9.000
12.000
15.000
18.000
BENDING ANGLE (DEGREES) (X10 ')

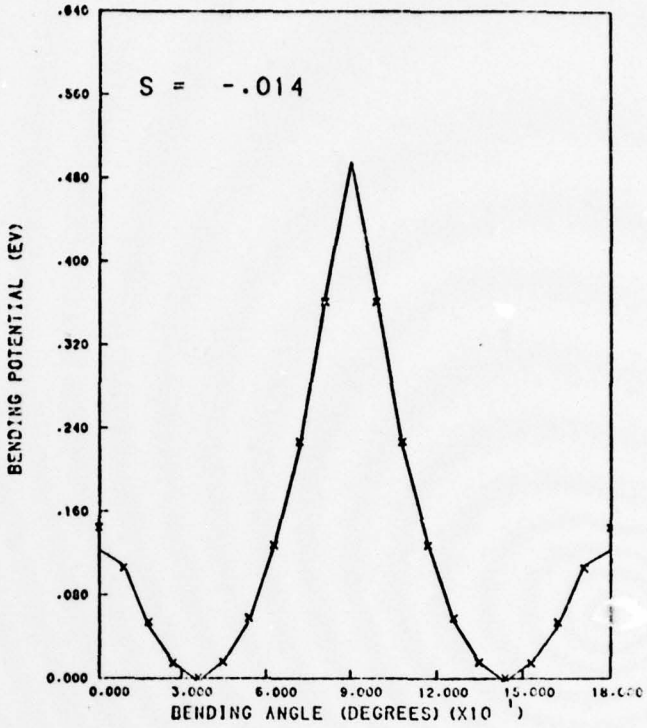
S = -.014
BENDING POTENTIAL (EV)
.640
.560
.480
.400
.320
.240
.160
.080
0.000
0.000
3.000
6.000
9.000
12.000
15.000
18.000
BENDING ANGLE (DEGREES) (X10 ')

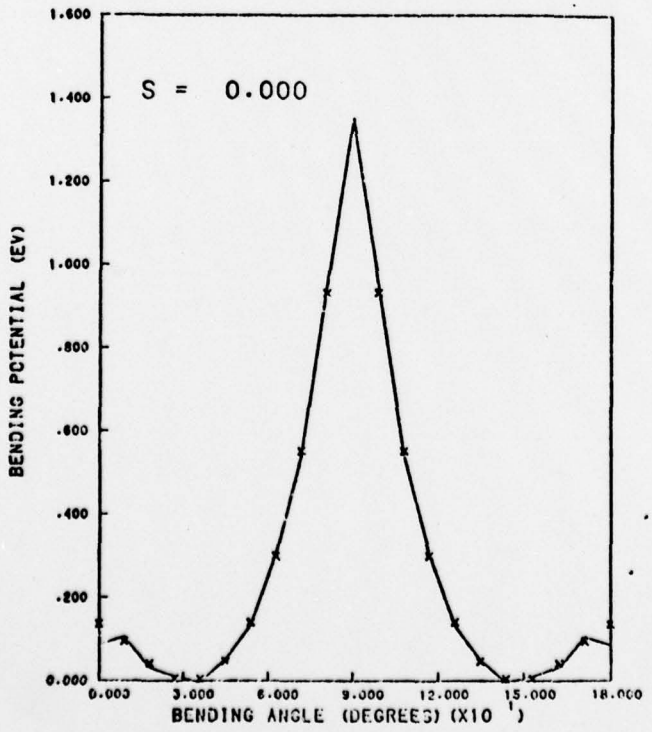
S = 0.000
BENDING POTENTIAL (EV)
1.600
1.400
1.200
1.000
.800
.600
.400
.200
0.000
0.000
3.000
6.000
9.000
12.000
15.000
18.000
BENDING ANGLE (DEGREES) (X10 ')

Figure 7

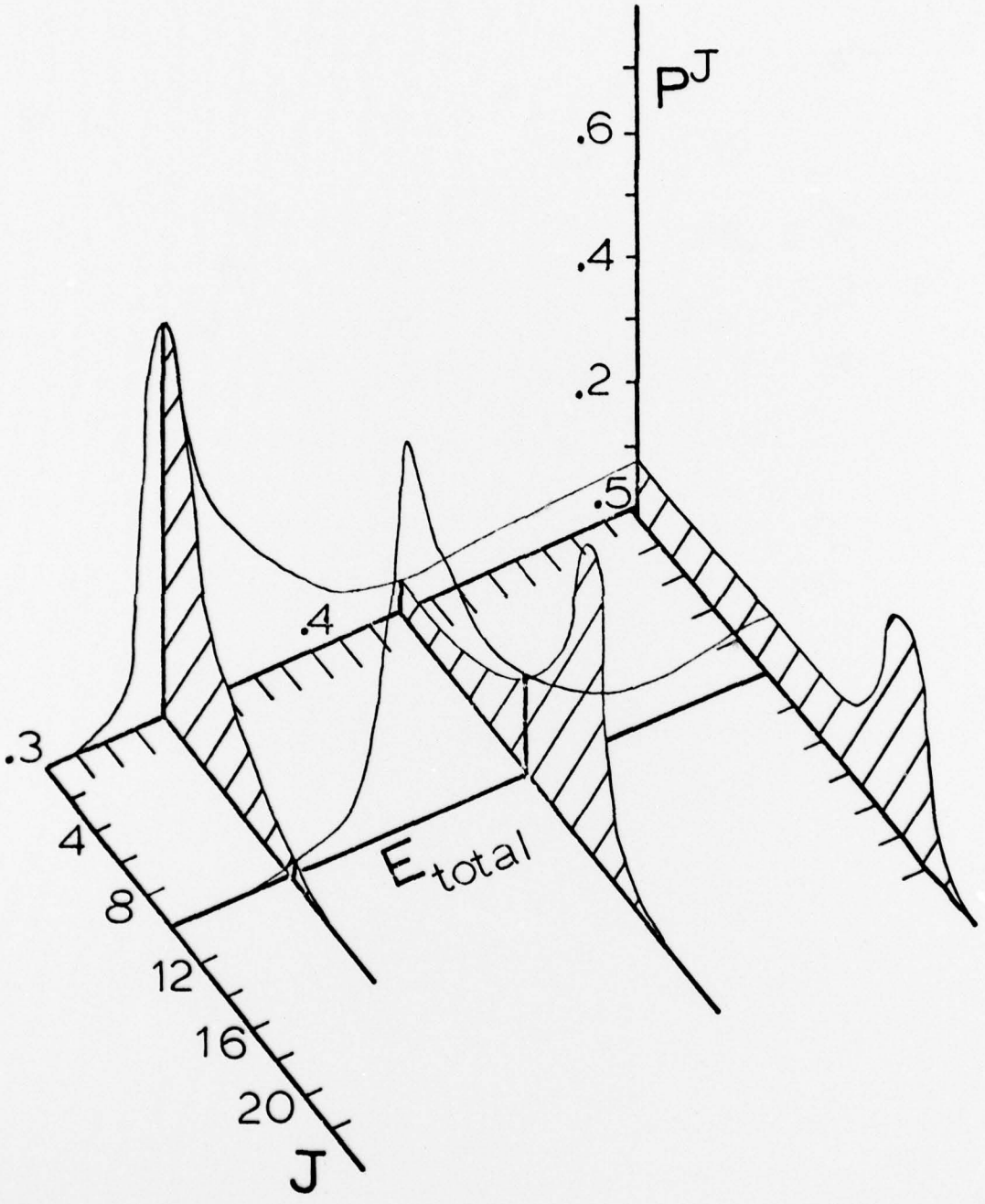

Figure 8

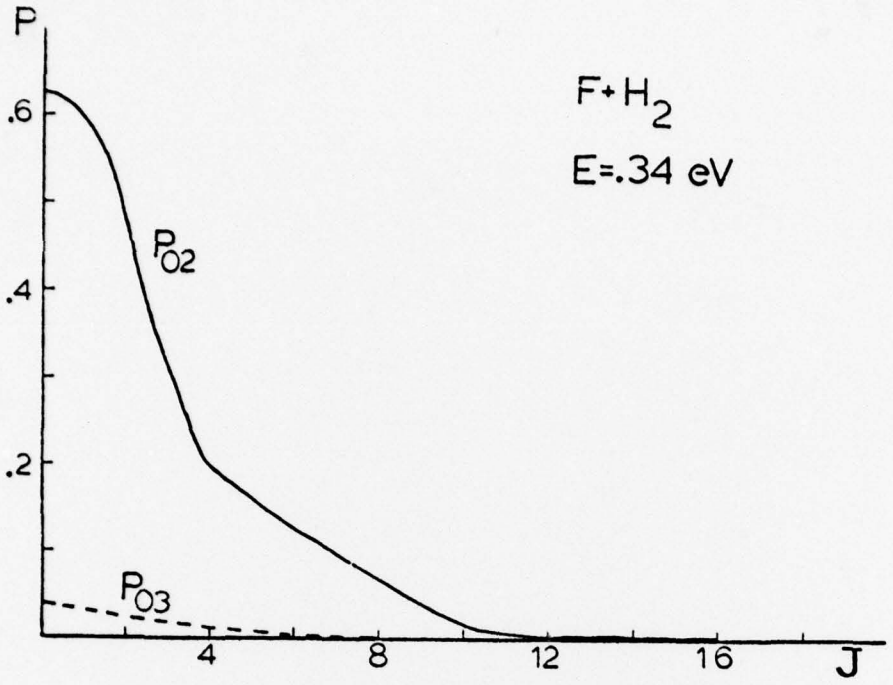
P
.6
.4
.2
F+H2
E=.34 eV
P02
P03
4
8
12
16
J

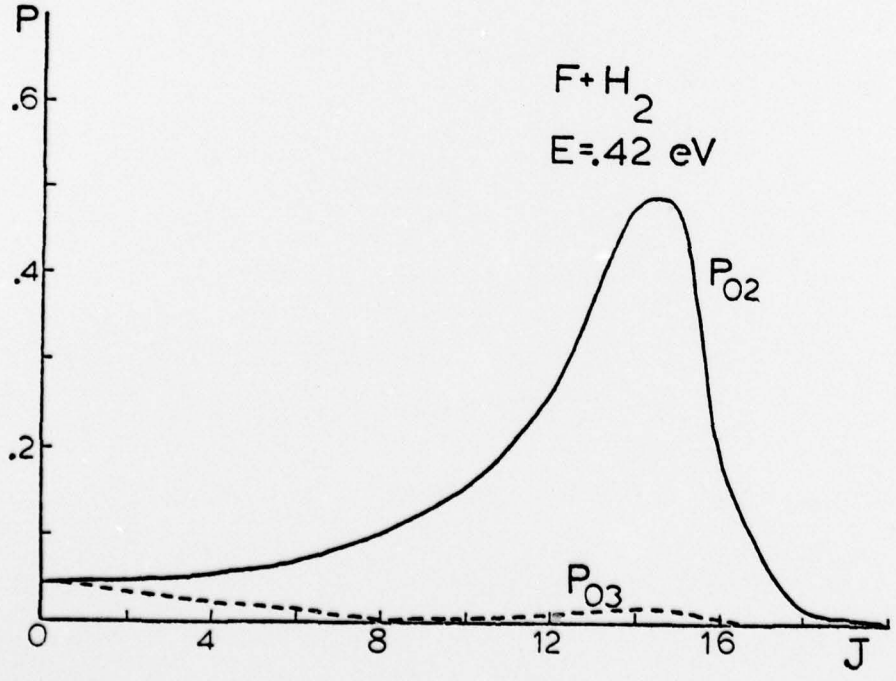
P
.6
.4
.2
F+H2
E=.42 eV
P02
P03
0
4
8
12
16
J

Figure 9

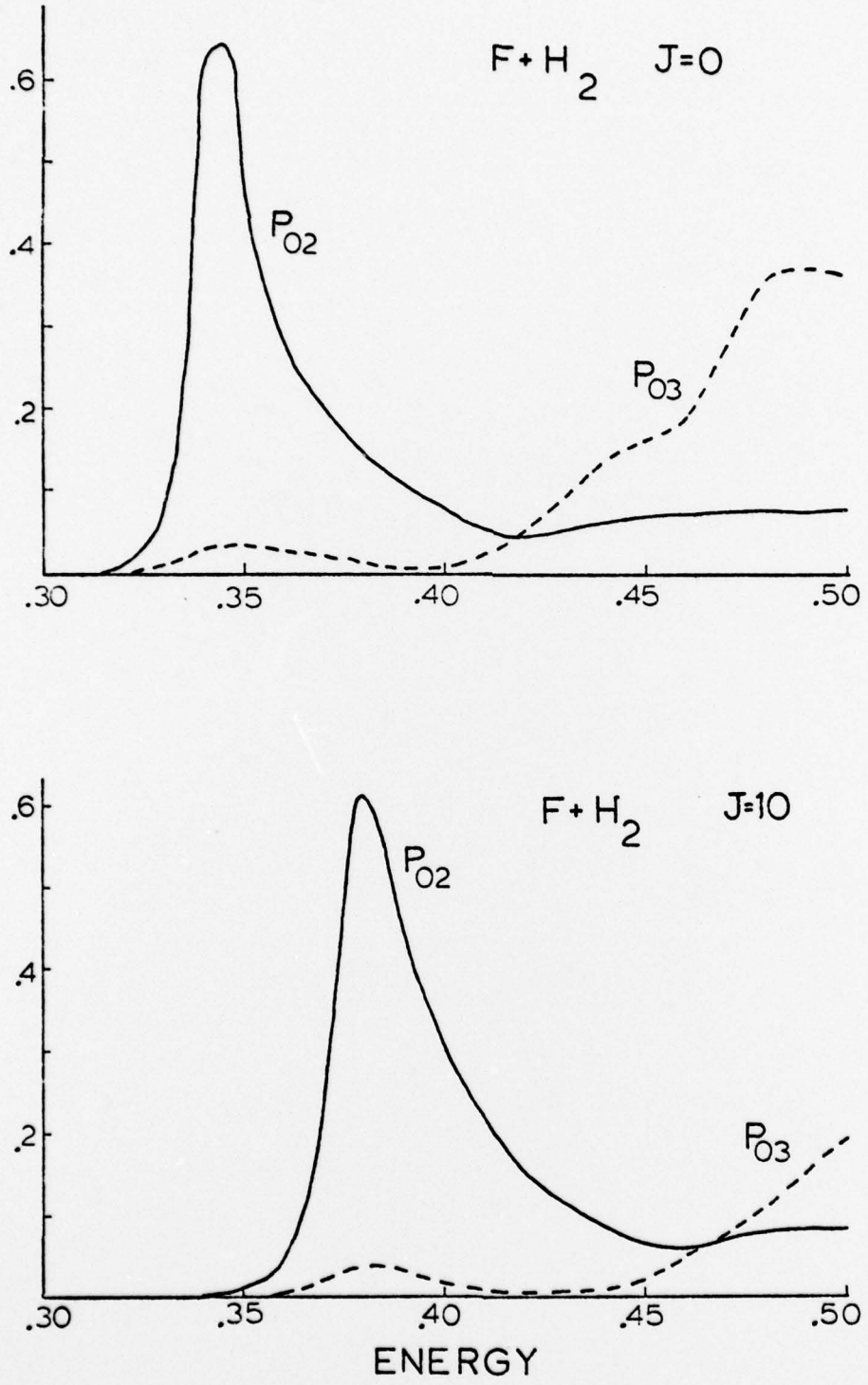
F + H2 J=0
P02
P03
.6
.4
.2
.30
.35
.40
.45
.50
F + H2 J=10
P02
P03
.6
.4
.2
.30
.35
.40
.45
.50
ENERGY

Figure 10

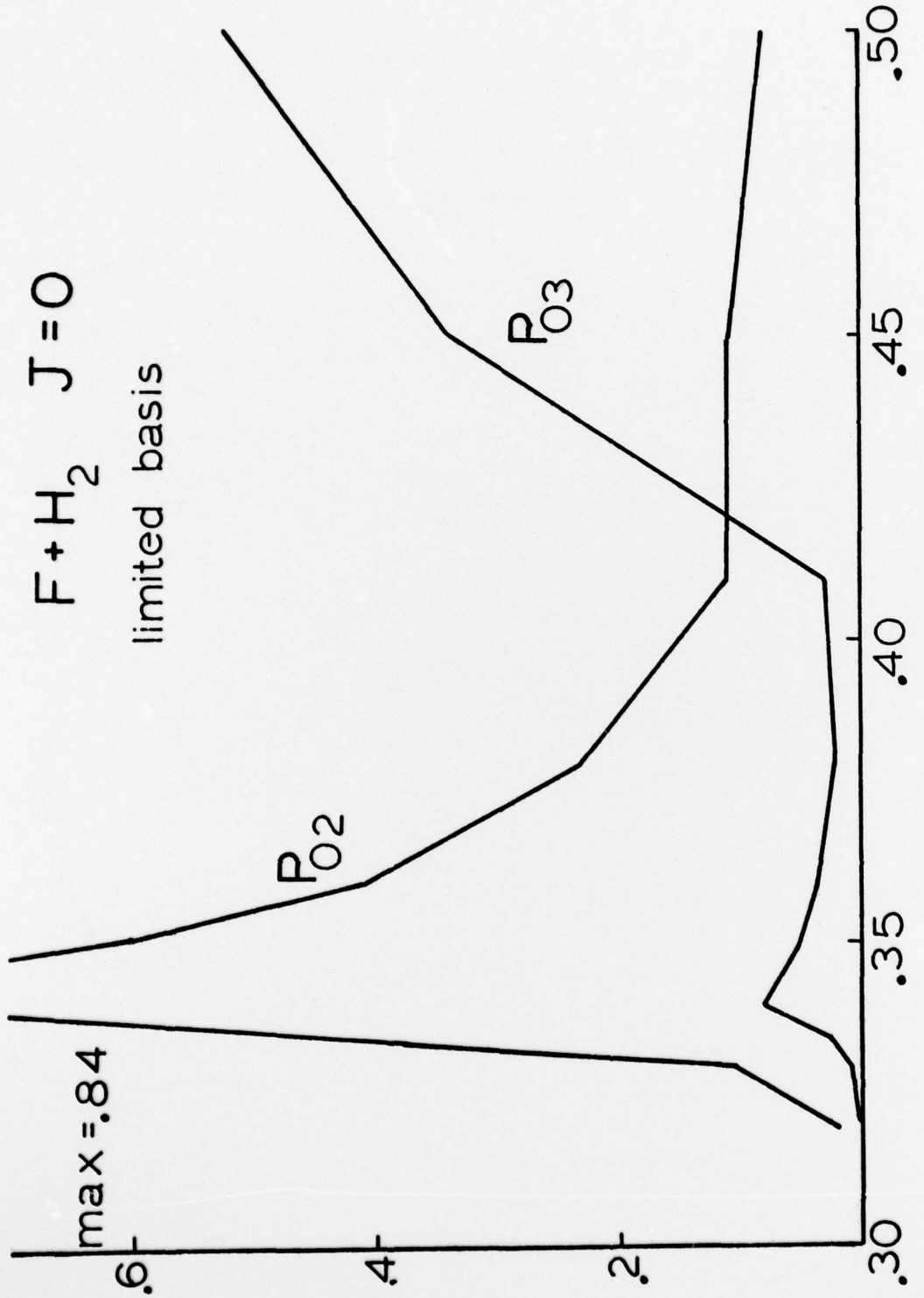

Figure 11

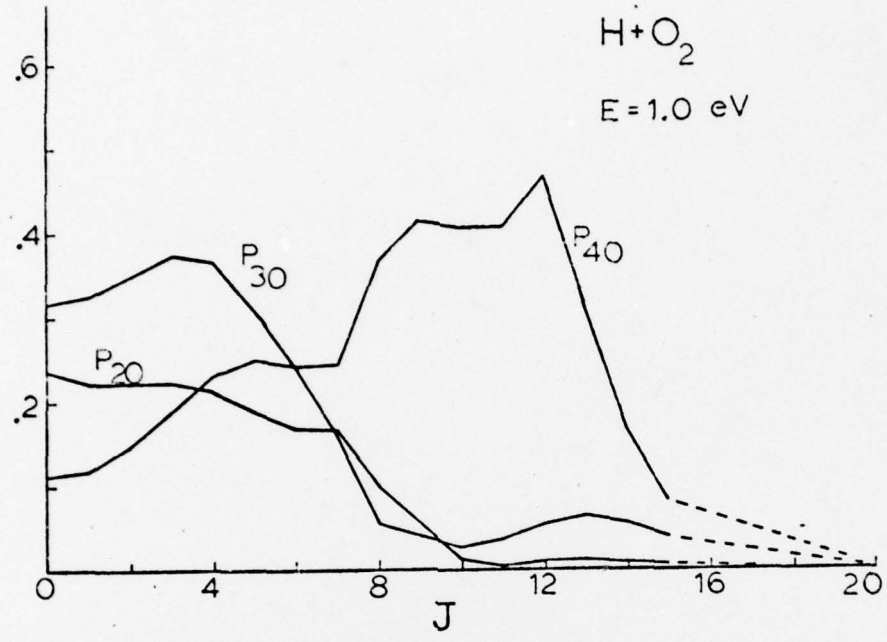
H+O2
E=1.0 eV
.6
.4
.2
P30
P40
P20
0
4
8
12
16
20
J

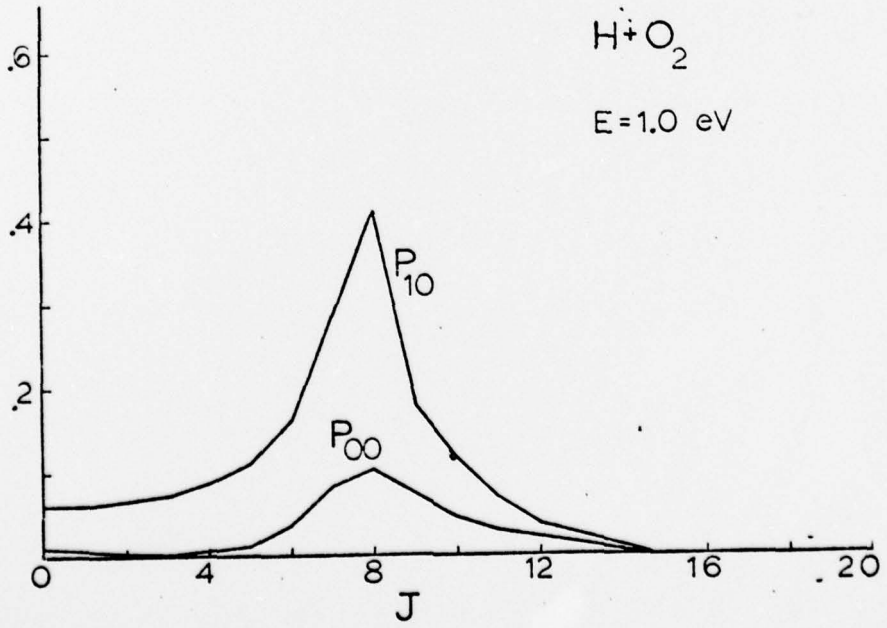
H+O2
E=1.0 eV
.6
.4
.2
P10
P00
0
4
8
12
16
20
J

Figure 12

Unclassified

SECURITY CLASSIFICATION OF THIS PAGE (When Data Entered)

REPORT DOCUMENTATION PAGE		READ INSTRUCTIONS BEFORE COMPLETING FORM
1. REPORT NUMBER 13600.2-CX	2. GOVT ACCESSION NO.	3. RECIPIENT'S CATALOG NUMBER
4. TITLE (and Subtitle) Computational Study of Chemical Reaction Dynamics: Quantum Study of Selected Atom-Diatomic Molecule Reactions Involving Hydrogen, Oxygen, and Nitrogen		5. TYPE OF REPORT & PERIOD COVERED Final Report: 1 Jun 76 - 31 May 78 6. PERFORMING ORG. REPORT NUMBER
7. AUTHOR(s) George Wolken, Jr.		8. CONTRACT OR GRANT NUMBER(s) DAAG29 76 C 0048
9. PERFORMING ORGANIZATION NAME AND ADDRESS Battelle Columbus Laboratories Columbus, Ohio 43201		10. PROGRAM ELEMENT, PROJECT, TASK AREA & WORK UNIT NUMBERS
11. CONTROLLING OFFICE NAME AND ADDRESS U. S. Army Research Office P. O. Box 12211 Research Triangle Park, NC 27709		12. REPORT DATE July 14, 1978 13. NUMBER OF PAGES 40
14. MONITORING AGENCY NAME & ADDRESS(if different from Controlling Office)		15. SECURITY CLASS. (of this report) unclassified 15a. DECLASSIFICATION/DOWNGRADING SCHEDULE

16. DISTRIBUTION STATEMENT (of this Report)

Approved for public release; distribution unlimited.

17. DISTRIBUTION STATEMENT (of the abstract entered in Block 20, if different from Report)

18. SUPPLEMENTARY NOTES

The findings in this report are not to be construed as an official Department of the Army position, unless so designated by other authorized documents.

19. KEY WORDS (Continue on reverse side if necessary and identify by block number)

20. ABSTRACT (Continue on reverse side if necessary and identify by block number)

The natural collision coordinate theory of quantum reactive scattering was generalized to reactions of the form AB+C in which the reaction intermediate could be nonlinear. An approximation to the NCC kinetic energy operator was employed which systematically reduces to that of Wyatt when applied to a linear intermediate. A scattering code developed previously was modified to compute the many additional terms required in the kinetic energy. The resulting code is the present state-of-the-art in the application of quantum reactive scattering theory to general bimolecular reactions.

DD FORM 1 JAN 73 1473 EDITION OF 1 NOV 65 IS OBSOLETE

Unclassified

13600.2-CX

20. ABSTRACT CONTINUED

The new code was tested by application to the H + H_2^* and F + H_2^* reactions, and then applied to the H + O_2^* combustion reaction. As will be seen below, many new results were obtained which should aid our understanding of microscopic processes, many of which are difficult to study experimentally.